

Composite Megacolumns

Testing Multiple, Concrete-Encased,
Hot-Rolled Steel Sections

Dario Trabucco, Jean-Claude Gérardy,
Congzhen Xiao & Donald Davies



Composite Megacolumns

Testing Multiple, Concrete-Encased, Hot-Rolled Steel Sections

Research Coordinator:

Council on Tall Buildings and Urban Habitat (CTBUH)

Dario Trabucco, Antony Wood & Eleonora Lucchese

Research Sponsor:

ArcelorMittal (AMBD)

Olivier Vassart, Nicoleta Popa, Jean-Claude Gérardy & Teodora Bogdan

Technical and Testing Partner:

China Academy of Building Research Technologies (CABR)

Congzhen Xiao, Tao Chen & Fei Deng

Engineering Partner:

Magnusson Klemencic Associates (MKA)

Donald Davies

October 2016

For more information, contact: *Dr. Dario Trabucco, CTBUH Research Manager, dtrabucco@ctbuh.org*



Research funded by:





Research Funded By:



Bibliographic Reference:

Trabucco, D.; Gérardy, J. C.; Xiao, C. & Davies, D. 2016. *Composite Megacolumns: Testing Multiple, Concrete-Encased, Hot-Rolled Steel Sections*. Chicago : Council on Tall Buildings and Urban Habitat.

Research Team: Teodora Bogdan, Tao Chen, Donald Davies, Fei Deng, Jean-Claude Gérardy, Brett Gourley, Eleonora Lucchese, Nicoleta Popa, Dario Trabucco, Olivier Vassart, Jingye Wang, Alex J. Wileg, Antony Wood, Congzhen Xiao
Editorial Support: William Miranda
Layout: William Miranda & Tansri Muliani

Published by the Council on Tall Buildings and Urban Habitat (CTBUH) in conjunction with ArcelorMittal

© 2016 Council on Tall Buildings and Urban Habitat

The right of the Council on Tall Buildings and Urban Habitat to be identified as author of this work has been asserted by them in accordance with sections 77 and 78 of the Copyright, Designs and Patents Act 1988.

All rights reserved. Apart from any fair dealing for the purposes of private study, research, criticism or review as permitted under the Copyright Act, no part of this publication may be reproduced, stored in a retrieval system or transmitted in any form by any means, electronic, mechanical, photocopying, recording or otherwise, without the written permission of the publisher.

Trademark notice: Product or corporate names may be trademarks or registered trademarks, and are used only for identification and explanation without intent to infringe.

Library of Congress Cataloging-in-Publication Data
A catalog record has been requested for this book

ISBN: 978-0-939493-53-1

Council on Tall Buildings and Urban Habitat

The Monroe Building
104 South Michigan Avenue, Suite 620
Chicago, IL 60603
United States
Phone: +1 312 283 5599 Fax: +1 844 823 9392
Email: info@ctbuh.org
www.ctbuh.org
www.skyscrapercenter.com



CTBUH Asia Headquarters Office

College of Architecture and Urban Planning, Tongji University
1239 Si Ping Rd, Yangpu District
Shanghai, China 200092
Phone: +86 21 6598 2972
Email: china@ctbuh.org



CTBUH Research Office

Iuav University of Venice
Dorsoduro 2006
30123 Venice
Italy
Phone: +39 41 257 1276
Email: research@ctbuh.org



Authors

Teodora Bogdan, *ArcelorMittal*
Tao Chen, *CABR*
Donald Davies, *MKA*
Fei Deng, *CABR*
Jean-Claude Gérardy, *ArcelorMittal*
Eleonora Lucchese, *CTBUH*
Nicoleta Popa, *ArcelorMittal*
Dario Trabucco, *CTBUH*
Olivier Vassart, *ArcelorMittal*
Antony Wood, *CTBUH*
Congzhen Xiao, *CABR*

Peer Review Panel

Simon Cloherty, *Robert Bird Group*
Bill Faschan, *LERA*
Craig Gibbons, *Arup*
Bao Lianjing, *ECADI*
Neville Mathias, *SOM*
John Peronto, *Thornton Tomasetti*
Andre Plumier, *ULg - PLUMIECS*
Dennis Poon, *Thornton Tomasetti*
Juneid Qureshi, *Meinhardt*
Ahmad Rahimian, *WSP Cantor Seinuk*
Tom Schlafly, *AISC*
Jinpeng Tan, *MCC CERl Architects and Engineers*
Aaron Wang, *CapitaLand*
Sugeng Wijanto, *GIS Gistama Intisemesta*

About the CTBUH

The Council on Tall Buildings and Urban Habitat (CTBUH) is the world's leading resource for professionals focused on the inception, design, construction, and operation of tall buildings and future cities. Founded in 1969 and headquartered at Chicago's historic Monroe Building, the CTBUH is a not-for-profit organization with an Asia Headquarters office at Tongji University, Shanghai; a Research Office at Luav University, Venice, Italy; and a Research & Academic Office at the Illinois Institute of Technology, Chicago. CTBUH facilitates the exchange of the latest knowledge available on tall buildings around the world through publications, research, events, working groups, web resources, and its extensive network of international representatives. The Council's research department is spearheading the investigation of the next generation of tall buildings by aiding original research on sustainability and key development issues. The Council's free database on tall buildings, The Skyscraper Center, is updated daily with detailed information, images, data, and news. The CTBUH also developed the international standards for measuring tall building height and is recognized as the arbiter for bestowing such designations as "The World's Tallest Building."



Council on Tall Buildings and Urban Habitat

www.ctbuh.org

www.skyscrapercenter.com

About the Research Sponsor: ArcelorMittal

With annual achievable production capacity of approximately 127 million tons of crude steel, and 222,000 employees across 60 countries, ArcelorMittal is the world's leading steel and mining company. With an industrial presence in over 20 countries, they are the leader in all major global steel markets including automotive, construction, household appliances and packaging, with leading research and development and technology, sizeable captive supplies of raw materials, and extensive distribution networks.

ArcelorMittal uses their researchers' expertise in steel to develop cleaner processes and greener products, including ultra-high-strength steels (UHSS) and Ultra-Low CO₂ Steelmaking (ULCOS), to make steel production more sustainable and help reduce both their own environmental impact and that of their customers.



ArcelorMittal

This document is the summary of the research on composite megacolumns. A complete description of the present research program, including all information and data of the experimental campaign can be found in the detailed report, titled *Performance and Capacity of Isolated Steel Reinforced Concrete Columns and Design Approaches*, available online at www.ctbuh.org/megacolumns or through the following QR code:



For brevity, some of the explanations and concepts required to fully understand the research have been removed from the present paper, but can be found in the complete research report, available at the link above.

Table of Contents

About CTBUH and ArcelorMittal	4
1.0 Research Executive Summary: Background and Overview	8
2.0 Laboratory Testing	10
2.1 Static Tests	10
2.2 Static Test Results	12
2.3 Quasi-static Tests	15
2.4 Quasi-static Test Results	18
2.5 Result Overview	21
3.0 Validation of Test Results with FEM and International Codes	22
3.1 FEM and Chinese JGJ Code Validation	22
3.2 FEM and Eurocode 4 Validation	24
4.0 Simplified Design Methods and Examples	28
4.1 Notation	28
4.2 Design Case Sections and Properties	29
4.2.1 Flange Layers of Rebar – Moment of Inertia	29
4.2.2 Flange Layers of Rebar – Plastic Moment	30
4.2.3 Web Layers of Rebar – Moment of Inertia	30
4.2.4 Web Layers of Rebar – Plastic Moment	31
4.2.5 Steel Profiles – Moment of Inertia	31
4.2.6 Evaluation of Effective Flexural Stiffness	32
4.2.7 Tables	36
5.0 Conclusions	46
References	48
Code References	48
List of Tables	49
List of Figures	50

1.0 Research Executive Summary: Background and Overview

The aim of this paper is to provide an overview on the developments and achievements of the research program carried out between August 2014 and December 2015 on composite megacolumns with encased, hot-rolled steel sections.

The project was supported and funded by ArcelorMittal (AMBD). The structural engineering firm Magnusson Klemencic Associates (MKA) provided background studies on comparative composite megacolumn construction projects, both within China and other international markets. The China Academy of Building Research (CABR) was engaged to develop the testing program for the subject columns. The Council on Tall Buildings and Urban Habitat (CTBUH) assumed the role of project coordinator.

There is an ongoing need to optimize construction materials and reduce the size of elements required within the structural systems of high-rise buildings. Minimizing the size of the vertical structural elements, without compromising the economic feasibility of projects and limiting their significant share on tall buildings' floor plans, is a consistent challenge. The use of composite structural elements, such as combining concrete and steel, along with higher grade materials within each, is a viable solution.

Currently, concrete filled tubes (CFT) or concrete filled continuous caissons built-up by welding heavy plates are the common structural solutions. Their main drawbacks include high costs, the need for skilled labor, complex connections, and requiring welding conditions for heavy plates, such as preheating and repairing.

Composite megacolumns considered in this research are defined as vertical structural systems with more than one hot-rolled steel section, longitudinal rebar and ties embedded in concrete, and they are subject to significant vertical loads and secondary bending moments from wind and seismic actions. They are believed to be a convenient solution in terms of structural behavior, cost, and constructability for the design of tall buildings, including towers over 300 meters tall.

Although codes and specifications do consider composite structural elements, they do not offer specific provisions on the

design of composite sections with two or more encased steel sections (AISC 2010 Specifications for instance).

The lack of knowledge on the axial, bending, and shear behavior of composite megacolumns, along with the resulting lack of clarity in the codes, leads to the need for experimental performance tests. These tests, and the resulting findings, suggest a simplified design approach and help develop numerical methods to describe the designs and to validate the results.

The laboratory tests took place between February and September 2015 within CABR Laboratories and the Laboratories of Tsinghua University, Beijing.

The column specimens' overall layout and geometry have been based on suggested sections, from MKA and others, of representative full scale composite columns considered for high-rise buildings. Overall dimensions of the representative full scale columns considered for this testing program are 1,800 by 1,800 millimeters, with a height of 9 meters at the Lobby level (base of the tower) and 4.5 meters at the typical floor.

The laboratory tests consisted of two sets of tests that attempt to define the axial load and moment (P-M) interaction curves of the representative columns at failure. Static tests were accomplished by applying 0%, 10%, and 15% eccentricity axial loads, on six 1:4 scaled specimens, until failure. Quasi-static tests were accomplished by applying 10% and 15% eccentricity axial loads with horizontal forces on four 1:6 scaled specimens, until failure.

Results are used to investigate the specimens' maximum capacity, displacements, stress distribution, ductility, and stiffness.

Experimental results are validated by finite element method (FEM) models developed by CABR and AMBD with Abaqus and Safir software, with the numerical values in accordance with the experimental values. FEM models allow also for a deeper insight on steel-concrete interaction forces and stress distribution.

Finally, simplified design methods based on European, Chinese, and US codes are suggested and the results are compared to the numerical and experimental values. Then, through three examples of application to selected megacolumn sections, the simplified methods are proven to be an effective and useful design tool.

The present paper has undergone a peer review process before official circulation, with feedback received from professionals on tall buildings, structural designers, and professors involved in the peer review panel.

A complete description of the present research program, including all information and data of the experimental campaign can be found in the extensive, detailed report, titled *Performance and Capacity of Isolated Steel Reinforced Concrete Columns and Design Approaches*, available at the following link and QR code:

www.ctbuh.org/megacolumns



2.0 Laboratory Testing

The aim of this section is to describe the laboratory testing performed between February and September 2015 within CABR Laboratories and the Laboratories of Tsinghua University, Beijing, with the purpose of quantifying the behavior of composite megacolumns under combined compression and bending conditions.

2.1 Static Tests

During the static tests, six 1:4 scaled specimens are tested to failure by applying a concentrated load with different eccentricities.

The total length of the specimens are 2,700 millimeters, with 450 by 450 millimeters square cross sections, simulating a megacolumn with a length of 9 meters and a 1,800 by 1,800 millimeters cross section, representative of a column located in a double-floor lobby. They all have the same configuration of four hot rolled HEM100 (120x106x12x20) steel sections encased in concrete, longitudinal rebar, and steel tie sets (see Figures 1 and 2). Studs are welded in one and two rows on the profiles inner flange, web, and outer flange (see Figure 3).

Figure 4 shows different stages of specimens' fabrication.

Selected materials are listed in Tables 1 and 2.

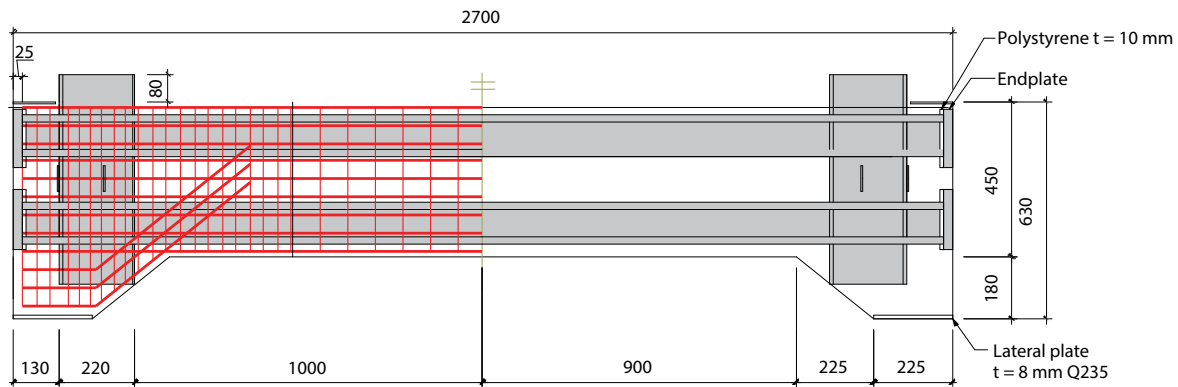


Figure 1. Static test specimens' steel layout – longitudinal. Source: CABR 2015

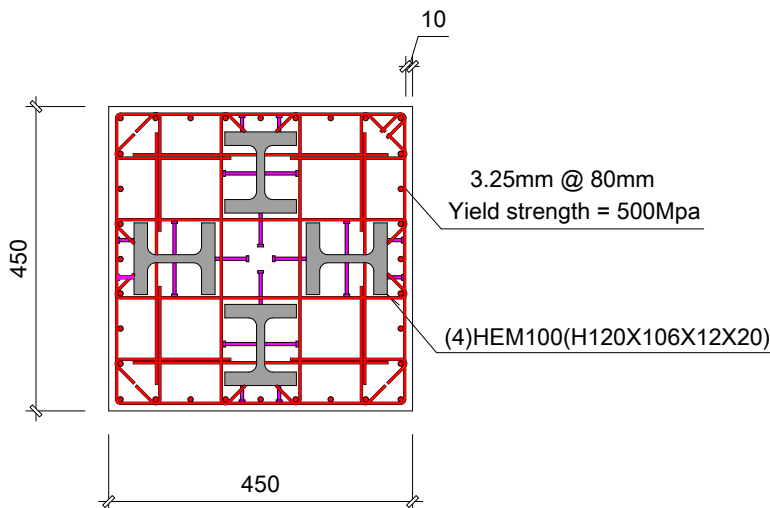


Figure 2. Static test specimens' steel layout – section. Source: CABR 2015

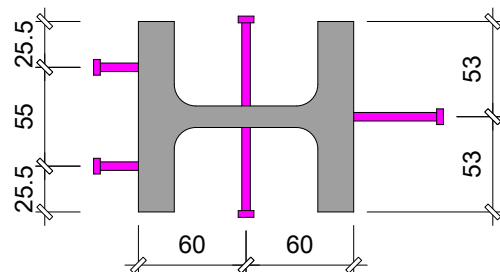


Figure 3. Static test specimens' shear studs layout. Source: CABR 2015



Figure 4. Specimen fabrication – static test, overview (a), bracket details (b), longitudinal bar details (c), and concrete mold (d). Source: CABR 2015

Concrete	C60 ($f_{ck} = 60$ MPa) according to Chinese Code, with 5 mm aggregate maximum size
Hot rolled jumbo sections	HEM100 (120x106x12x20) ASTM A572 Gr.50 / S355 ($f_{yk} = 355$ MPa = 50ksi)
Longitudinal reinforcement	Ø 8 mm HRB400 (ASTM A615), ($f_{yk} = 400$ MPa)
Stirrups	Ø 3.25 mm @ 80 mm HRB500 ($f_{yk} = 500$ MPa)
Shear studs	Ø 6 mm x 25 mm Nelson headed studs, ASTM A108 @ 144 mm O. C. Ø 5 mm x 20 mm Nelson headed studs, ASTM A108 @ 144 mm O. C. Grade 4.8

Table 1. Static test selected materials.
Source: First Methodological Report 2014

Specimen ID	Concrete cubic strength (MPa)	Concrete axial strength (MPa)	Yield strength of steel section flange* (MPa)	Yield strength of steel section web* (MPa)	Yield strength of longitudinal bar (MPa)	Yield strength of transverse bar (MPa)
E00-1	61.2	61.2	408	523	438	$f_{3.25} = 59$ MPa $f_{4.80} = 438$ MPa
E00-2	56.6	55.0	398	411		
E10-1	60.9	56.4	423	435		
E10-2	72.8	59.2	383	415		
E15-1	66.1	57.2	377	404		
E15-2	67.6	56.3	389	405		
Average	64.8	57.6	396	432	-	-

* Material strength for steel sections are provided by ArcelorMittal

Table 2. Material strengths for static tests.

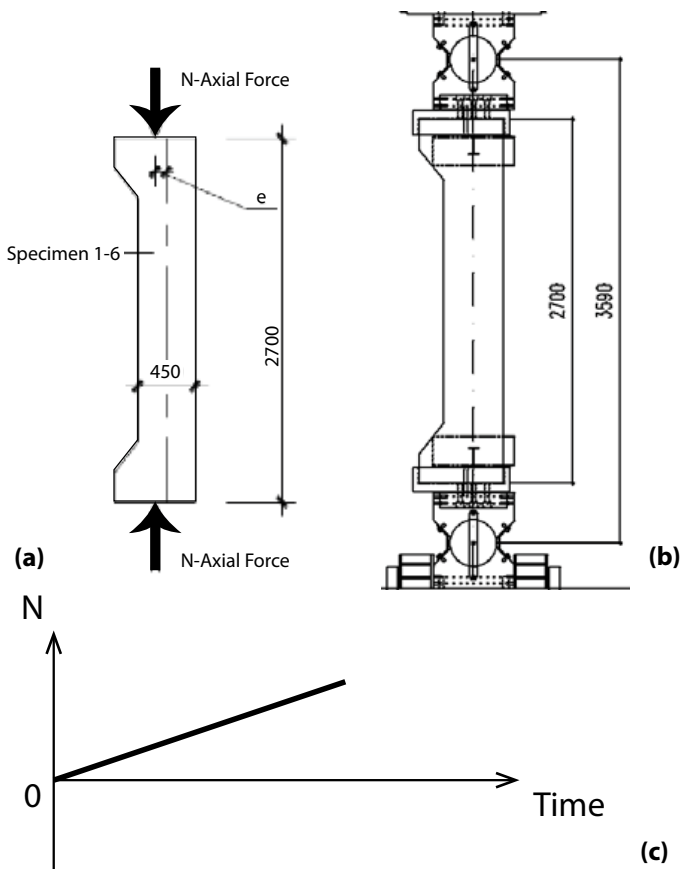


Figure 5. Static test setup (a), static test boundary condition (b), and static test axial load time history (c). Source: CABR 2015

Axial force is applied to the ends of the specimens with assigned eccentricity: two specimens are subjected to pure axial load (0% eccentricity) (E00-1 and E00-2), and two specimens are subjected to an axial load with 10% eccentricity (E10-1 and E10-2), two specimens are subjected to an axial load with 15% eccentricity (E15-1 and E15-2) (see Figure 5a).

A bottom hinge is fixed on the ground to prevent the specimens from horizontal displacements. A top hinge and bottom hinge allow rotation of the specimen extremity. It is connected to a transition beam restricting horizontal displacements and to the vertical actuator (see Figures 5b and 6).

The loading rate is set as slow, to prevent dynamic effects. Loads are increased gradually until failure of the specimen (see Figure 5c).

The data in this test program include measuring the strain on the profiles, longitudinal bars, ties and concrete surface, and



Figure 6. Static tests setup in lab. Source: CABR 2015

determining the relative displacement on concrete-steel profile interfaces. Strain sensors are placed on four sections of each specimen (see Figure 7).

The displacement sensor consists of two parts: a slide rheostat and a steel box. The slide rheostat is stuck on the surface of the steel section, surrounded by the steel box and the steel box is surrounded by concrete. During the test, the slide rheostat will move with the steel section and the box will move with the concrete, so the relative displacement can be detected.

2.2 Static Test Results

The static test results confirm the composite megacolumn expected behavior, and provide additional evidence of vertical and lateral displacements, curvature and ductility, axial and bending stiffness, and relative displacements between steel sections and concrete.

As the axial load increases, cracks develop; at first vertically, when the profile flanges are close to the concrete surface and the concrete is under tension, and then horizontally, when the specimen is reaching failure. Horizontal deflections of the specimens occur on E10 and E15 and, when the deflections

are large, axial load decreases and the test stops (see Figures 8 and 9).

On purely axial specimens, the first load drop is registered after the maximum axial load is reached. The axial load decreases as

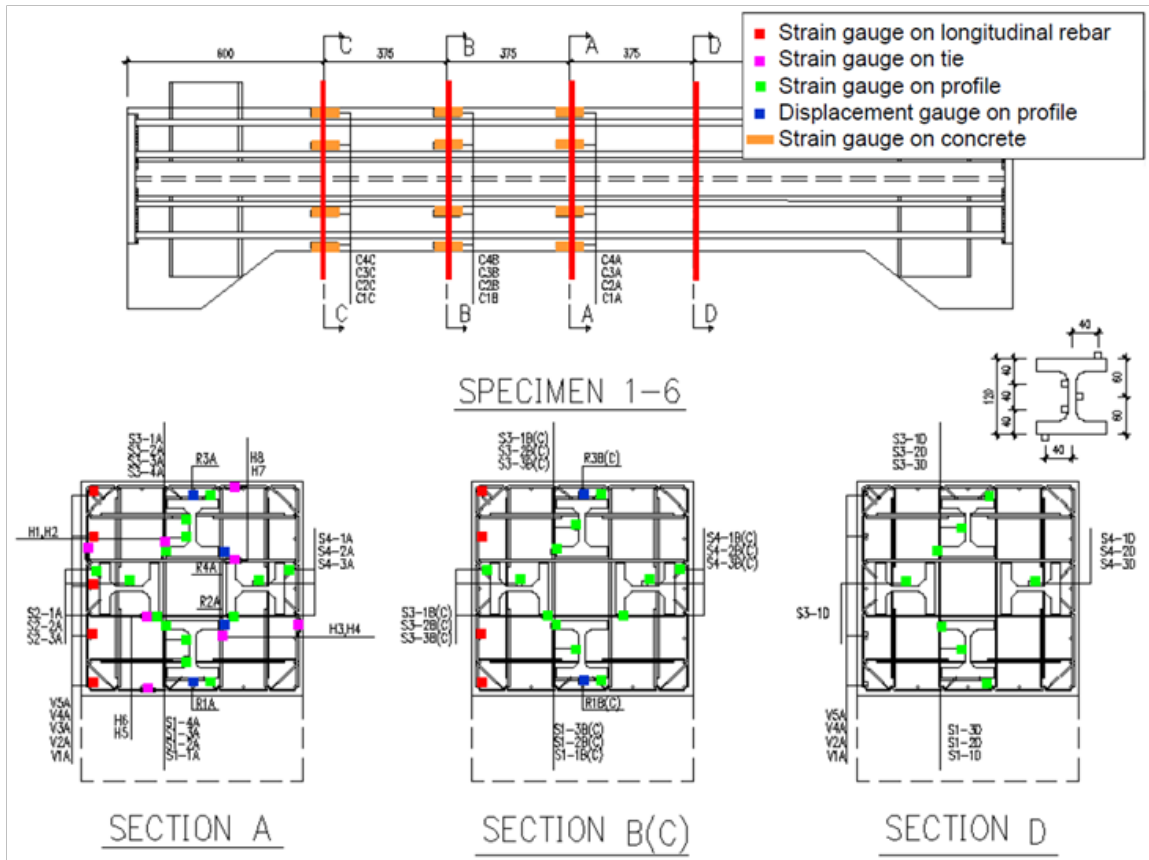


Figure 7. Static test configuration of strain and displacement gauges. Source: CABR 2015

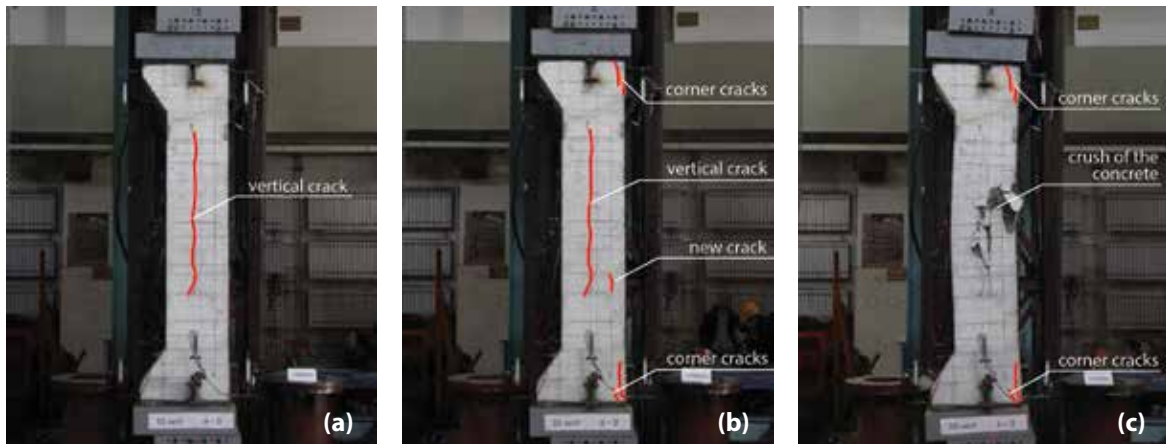


Figure 8. Test procedures – 70% of the maximum load (a), after the maximum load (b), and failure mode (c).

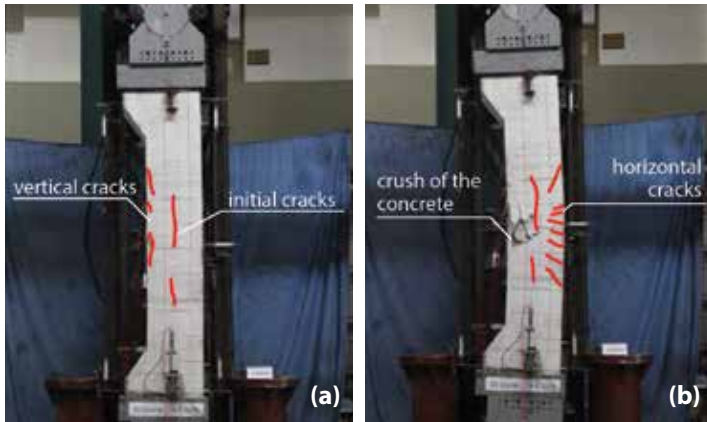


Figure 9. Crack development of specimens subjected to eccentric loads – 70% of the maximum load (a) and failure mode (b).

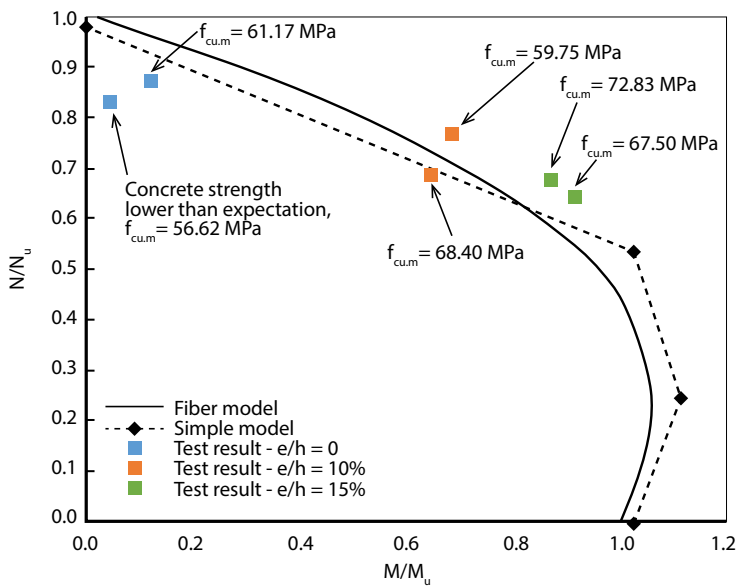


Figure 10. Theoretical and real interaction curve obtained by static tests.

the vertical deflection develops and the eccentricity increases. The second load drop occurs when the column fails, when sudden, significant deflections and damage occur. Eccentric specimens do not experience a sudden drop of applied load, as the axial load gradually decreases after the peak point. Meanwhile, the horizontal deflection and concrete damage continuously develop, especially on areas of the concrete under tension at the mid height of the specimen.

On purely axial specimens, buckling of the longitudinal rebar and breakage of ties are observed.

Specimen ID	Mu (kNm)	Nu (kN)
E00-1	142	17,082
E00-2	52	15,325
E10-1	803	14,360
E10-2	767	13,231
E15-1	1,076	12,041
E15-2	1,026	12,759

Table 3. Ultimate axial load and bending moment obtained with static tests.

Steel profiles yield, but do not buckle. No significant deformations of the profiles are registered.

The N-M interaction diagram is a graphical summary of the tests, represented as curve or surface, outlined by the axial load (N) and the bending moment (M), with the objective to capture the maximum cross-section strength. When the axial load and bending moment values are reported (see Table 3), they are used to produce an N-M diagram, and the experimental interaction curve is obtained (see Figure 10).

In Figure 10, the experimental interaction points correspond with the simplified interaction curve (according to Plumier method, et al.) and with the fiber model curve (programmed by CABB; refer to the *Performance and Capacity of Isolated Steel Reinforced Concrete Columns and Design Approaches* report: www.ctbuh.org/megacolumns).

Interaction curves are calculated using the average material strengths of the test specimens, which result in a divergence between the curves and the recorded data points. For specimens subject to eccentric loads, test results show good convergence with the curves. For specimens subject to axial loads, test results are smaller than predictions given by both the fiber model and the simplified method. Reasons for this difference includes: 1) concrete strengths of the two specimens are lower than the average value of six, and 2) the calculated results have not considered buckling effects or the $P-\Delta$ effects yet. Detailed procedures of determining the buckling and $P-\Delta$ effects are illustrated in the last chapter of this report. The composite columns do not reach the design value for axial load. One of these reasons could be because the concrete is crushing is outside the confined zone and the

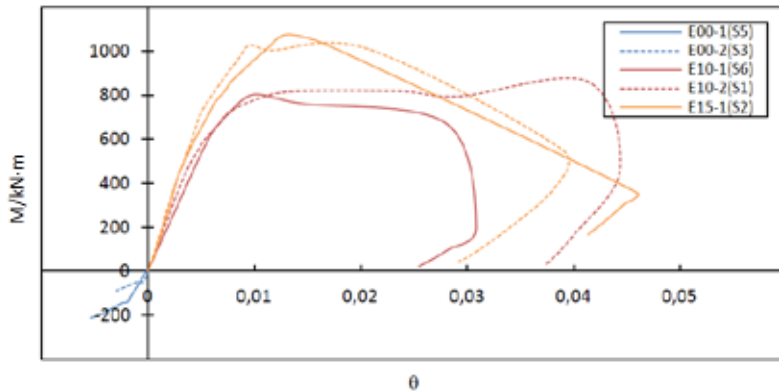


Figure 11. Moment vs. rotation of mid-section for eccentric specimens on static test.

Specimen ID	Vertical deflection at ultimate capacity (mm)	Horizontal deflection at ultimate capacity (mm)
E00-1	4.07	-7.78
E00-2	3.43	-2.84
E10-1	3.55	10.97
E10-2	3.46	12.95
E15-1	2.79	20.12
E15-2	2.70	12.30

Table 4. Vertical and horizontal displacement at ultimate axial load for static test.

concrete crushing strains outside the stirrups is below the design value of 3.5×10^{-3} .

Figure 11 shows the bending moment and rotation in the mid-section of the specimens. In this instance, the bending moment of the mid-section is constant as the curvature develops. The slopes of the curves become smaller with the increase of rotation, suggesting that the bending stiffness decreases as the load increases.

The area under the “moment vs. rotation” curve is a reflection of absorbed energy of the mid-section.

Thus, the static testing findings suggest that the ductility of the columns, in terms of the “moment vs. rotation” curve, have the potential to be excellent for columns with an eccentricity ratio less than 15% and above, as the ductility increases with the increasing eccentricity ratio. The second part of the testing program attempts to consider this ductility of the megacolumns under hysteretic loading.

While the modulus of elasticity between the rebar and steel profiles vs. the concrete is different, the initial assumption is that plane sections would remain this way until the point of system failure. Observations from strain gages within the test specimens, during the pure axial static testing, verify that the longitudinal rebar and steel sections remain elastic when purely axial specimen reach maximum capacity. The onset of failure started with the yielding of the concrete in compression, prior to reaching the steel yield strains. On eccentric specimen, longitudinal rebar and steel sections yield before it reaches maximum capacity.

The strain distribution of the mid section validates the “Plane Section Assumption” in this phase of the test.

For specimen materials and geometrical properties, reference values are shown on Table 1. Vertical deflection and horizontal displacements are reported in Table 4.

For stiffness reduction lease, refer to Section 4.2.6 on page 32.

As the eccentricity of the load increases, the slippage between concrete and steel sections also increases. As the sections are located further from the mid-span, higher slippage is registered. The maximum slippage for each specimen is considered low enough in order to validate the Plane Section Assumption for 10% eccentric specimen. With 10% eccentricity, maximum slippage for section B and section C is 2.22 millimeters and 1.19 millimeters, respectively; with 15% eccentricity, maximum slippage for section B and section C is 5.22 millimeters and 4.43 millimeters, respectively (see Figure 7 for section locations).

2.3 Quasi-static Tests

During quasi-static tests, four 1:6 scaled specimens are tested until failure by applying a concentrated vertical load and cyclic horizontal load. The behavior, including the capacity, deformation capacity, and hysteretic performance of the specimens under simulated seismic loads, are examined according to different eccentricities.

Four identical specimens, at a 1:6 scale, are built at a 1,900 millimeters height, with a square cross section of 300 by 300

millimeters. The shape is dictated by the simulation of a beam-column joint. Therefore, the symmetrical specimen is made of two parts: the upper and the lower specimens. Four W-steel sections ($h \times b \times t_w \times t_f = 80 \times 70 \times 12 \times 12$ mm) are vertically embedded in concrete, and two, horizontal W-steel beams ($140 \times 73 \times 4.7 \times 6.9$ mm) are welded to the vertical profiles (see Figure 12). Longitudinal steel bars and ties are included; shear studs are welded on the steel profile flanges

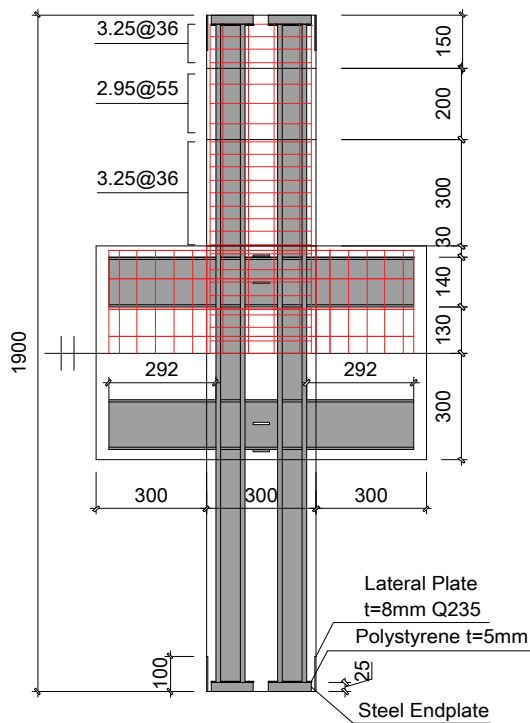


Figure 12. Quasi-static test specimens' steel layout – longitudinal.
Source: CABR 2015

Concrete	C60 ($f_{ck} = 38.5$ MPa) according to Chinese Code, with 5 mm aggregate maximum size
Hot rolled jumbo sections	Horizontal: 140x73x4.7x6.9 mm Vertical: HEM80 (80x60x12x12 mm) S235 ($f_{yk} = 235$ MPa = 34 ksi)
Longitudinal reinforcement	$\varnothing 6 / 8$ mm HRB400 (ASTM A615), ($f_{yk} = 400$ MPa)
Stirrups	$\varnothing 3.25$ mm @ 36 mm HRB500 ($f_{yk} = 500$ MPa)
Shear studs	$\varnothing 5$ mm x 25 mm Nelson headed studs; ASTM A108 @ 150 mm O. C $\varnothing 5$ mm x 15 mm Nelson headed studs; ASTM A108 @ 150 mm O. C Grade 4.8

Table 5. Quasi-static test selected materials.

and web, allowing their geometry to have appropriate concrete cover (see Figures 13, 14, and 15).

Selected materials are listed in Table 5, 6a, and 6b.

Axial force with 10% eccentricity is applied to specimens D10-1 and D10-2, and a 15% eccentricity axial force is applied to specimens D15-1 and D15-2, to account for the diversity in

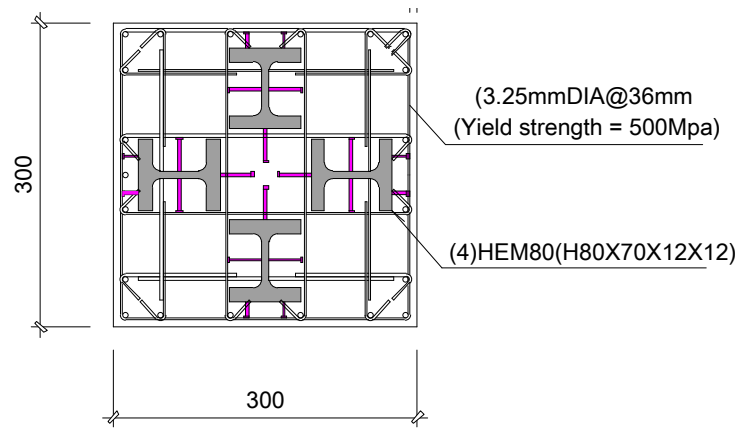


Figure 13. Quasi-static test specimens' steel layout – section.

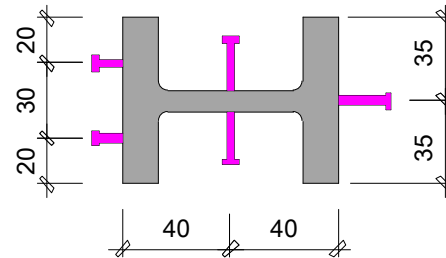


Figure 14. Quasi-static test specimens' shear stud layout.

Specimen ID	Block ID	Ultimate load (kN)	Compressive strength (MPa)	Average strength (MPa)
D10-1	1	1,506	67	70
	2	1,609	72	
	3	1,614	72	
D10-2	1	1,643	73	70
	2	1,609	72	
	3	1,489	67	
D15-1	1	1,686	75	76
	2	1,769	79	
	3	1,687	75	
D15-2	1	1,490	66	67
	2	1,559	69	
	3	1,506	67	

Table 6a. Strength of the concrete.

Material	Yield strength (MPa)	Ultimate strength (MPa)
Steel section	457	603
Longitudinal reinforcement (Ø 8 mm)	459	689
Longitudinal reinforcement (Ø 6 mm)	367	584
Transverse reinforcement	572	638
Shear stud	320	400

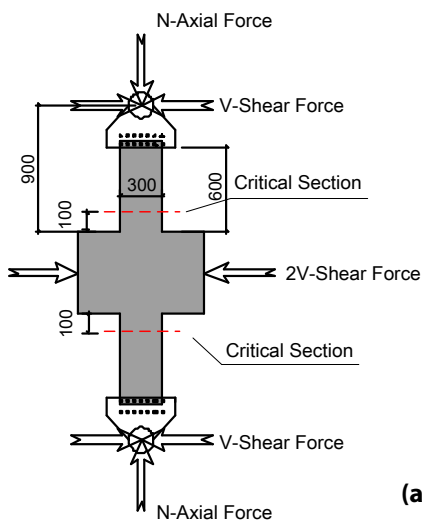
Table 6b. Strength of steel sections, reinforcement, and shear stud.

materials and fabrication. Horizontal force is applied at the mid-height of the specimens. Transverse load (V) is equal to two times the horizontal end reaction on the top and bottom of the specimens (see Figure 16a).

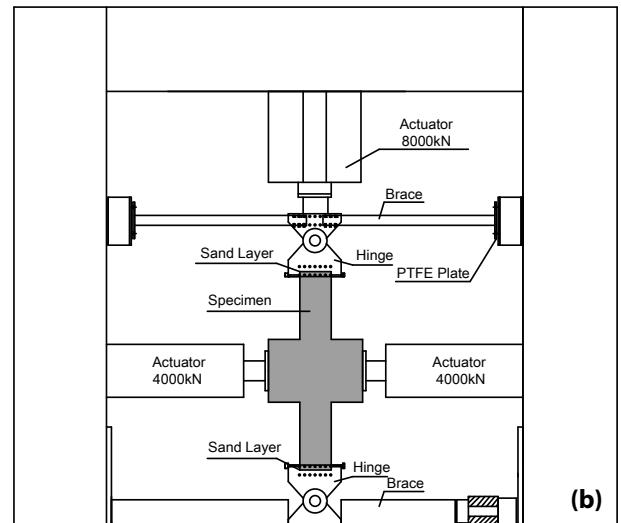
A bottom hinge is placed on the ground and a top hinge is installed on the top of the specimen, connecting it to the vertical actuator. Both the hinges are fixed by a frame that



Figure 15. Specimen fabrication – quasi-static test. Source: CABR 2015



(a)



(b)

Figure 16. The quasi-static test setup (a) and quasi-static boundary condition (b).



Figure 17. Quasi-static set up in lab. Source: CABR 2015

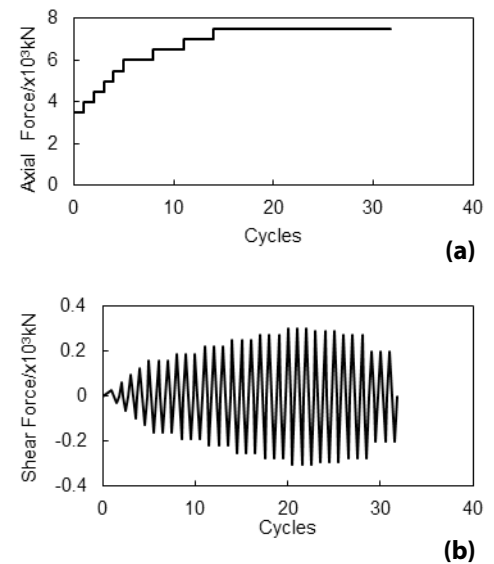


Figure 18. Quasi-static test axial load history (a) and the quasi-static test horizontal load history (b).

restricts horizontal displacements, as well as out-of-plane displacements (see Figures 16b and 17).

As shown in Figure 18, axial load slowly increases until it reaches the gravity load. Then, the axial load and the transverse load are increased proportionally. The axial load is increased by 500 kN steps, and the lateral load is applied cyclically, while keeping the axial load constant.

Displacement and strain through sensors, located close to the beam-column connection on the lower and upper column specimens, are measured in this program. The test sensors are shown in critical sections I and II (see Figure 19).

2.4 Quasi-static Test Results

The quasi-static test results confirm the column capacity and ductility of the static test results. The hypothesis on the static tests, known as the Plane Section Assumption, is verified within the 15% eccentricity ratio. The ability to dissipate energy is shown by stable and round hysteretic curves, without a large dependence on the eccentricity ratio.

Like the static tests, initial vertical cracks occur first on the face of the column. Then, the cracks and the damage of the concrete concurrently increase with the loads. In compression-controlled

flexural patterns, all of the specimens fail with severe damage at the corners of the concrete. This damage is believed to be caused by compressive strain of the specimens, rather than by the tensile strength. Despite the damage to the concrete cover, the core concrete remains intact because of the confinement effect provided by the steel sections. The concrete core confinement prevents the steel sections from buckling.

Rotation of the beams is recorded during the test, which are asymmetric due to fabrication errors and material diversities (see Tables 7 and 8). Note that some of the displacement sensors were damaged during the test, so measuring the vertical displacement at the ultimate capacity level was not possible for every specimen.

Local buckling of longitudinal rebar and breakage of the transverse ties are detected.

The ultimate bending moment capacity and axial load capacity are shown on the interaction curve (see Figure 20). This interaction curve is calculated based on fiber model, where the average tested material strength is used (refer to the *Performance and Capacity of Isolated Steel Reinforced Concrete Columns and Design Approaches* report: www.ctbuh.org/megacolumns). Static test results have been scaled to conform to the quasi-static test. The curve shows that the static and quasi-static tests are in accordance with the expected capacity.

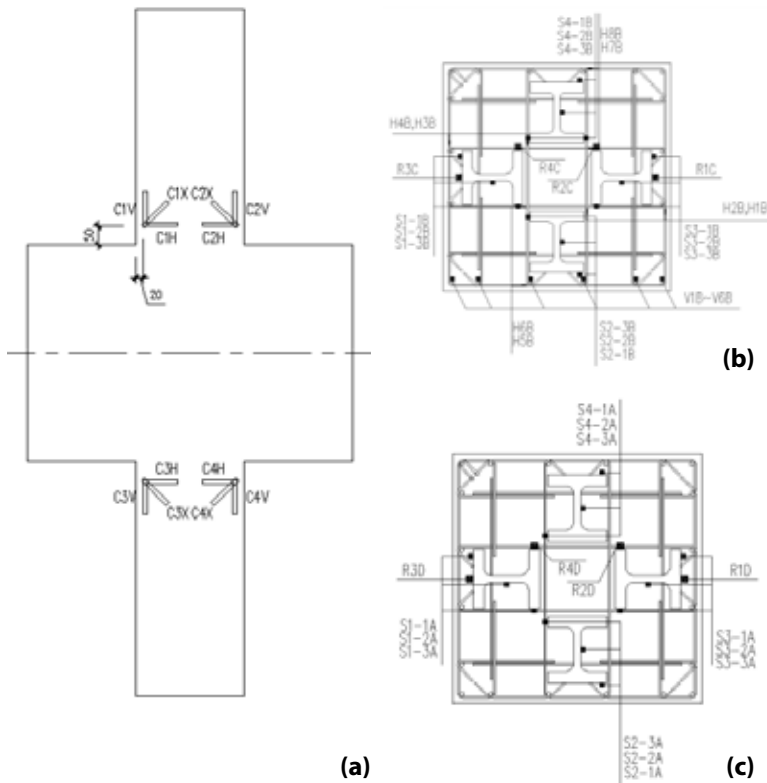


Figure 19. Quasi-static test sensors on the concrete (a), sensors on critical section I (b), and sensors on critical section II (c).

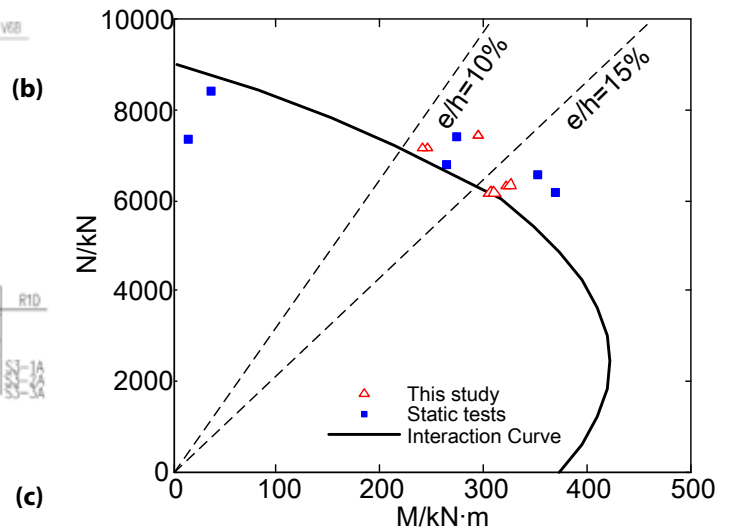


Figure 20. Theoretical and real interaction curve obtained by static and quasi-static tests.

Specimen ID	Direction	Vertical deflection at ultimate capacity (mm)	Horizontal deflection at ultimate capacity Average (mm)	Rotation Average
D10-1	Upper	-	12.14	1/74
	Lower	-	12.16	1/74
D10-2	Upper	7.07	10.18	1/88
	Lower	-	10.21	1/88
D15-1	Upper	5.40	13.65	1/66
	Lower	-	13.94	1/65
D15-2	Upper	5.19	12.55	1/72
	Lower	-	13.17	1/68

Table 7. Vertical and horizontal displacement at ultimate axial load for quasi-static test.

Actual eccentricities are larger than theoretical ones because of the second order effect.

The capacities of the 1:4 scaled specimens are transferred to capacities of the 1:6 scaled specimens.

Figure 21 shows the hysteretic curves, which show the relation between horizontal load and displacements. The data has been adjusted to account for the horizontal displacements,

Specimen ID	Direction	M_u (kNm)	N_u (kN)
D10-1	Upper	293	7,426
	Lower	322	7,427
D10-2	Upper	249	7,191
	Lower	242	7,189
D15-1	Upper	303	6,152
	Lower	308	6,154
D15-2	Upper	322	6,312
	Lower	324	6,312

Table 8. Ultimate axial load and bending moment obtained with quasi-static tests.

determined by the specimen deformation and the rigid rotation of the beam-to-column connection. The curves for the lower and upper column of specimen D10-1 and D10-2 are almost identical (see Figure 21a), but for D15-1 and D15-2 the curves are dissimilar because the specimens rotate counter-clockwise during the test (see Figure 21b).

The resulting curve is a cyclic curve, and the area included within the hysteretic curves represents the energy dissipation

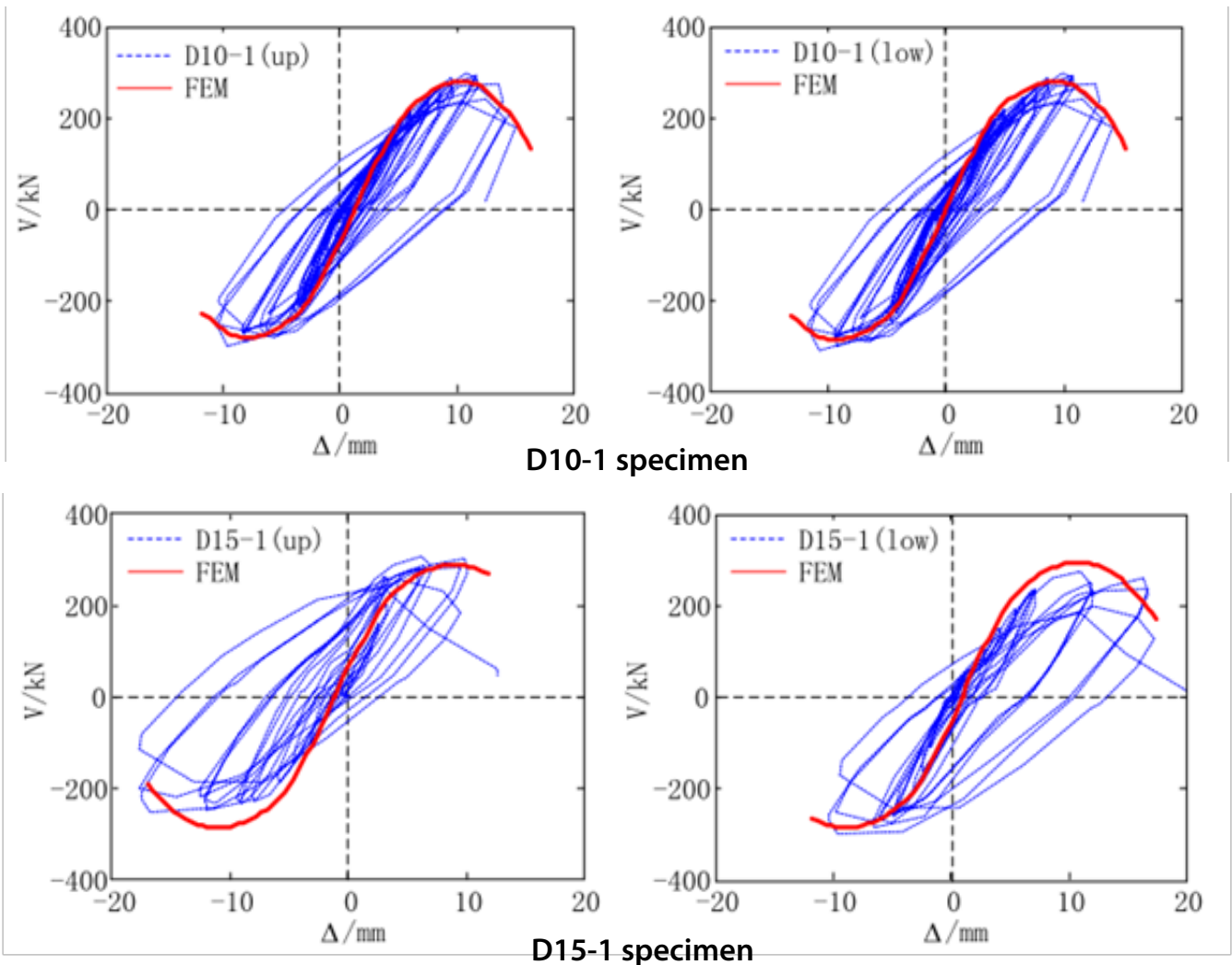


Figure 21. Hysteretic curves for D10-1 (a) and D15-1(b) specimens.

of the specimen. Hysteretic curves are round and stable, suggesting good energy dissipation, which is a very important aspect when evaluating the seismic performance of a composite column.

The area enclosed by the hysteretic curve can be represented by integrating the product of the load and displacement under different load levels. When the lateral displacement grows, materials yield and friction between the materials consume energy. Therefore, energy consumption increases, as does the lateral displacement (see Figure 22).

For specimens tested with 10% eccentricity until failure, strain distribution of concrete and steel section is linear, so the Plane Section Assumption can be verified. For specimens tested with

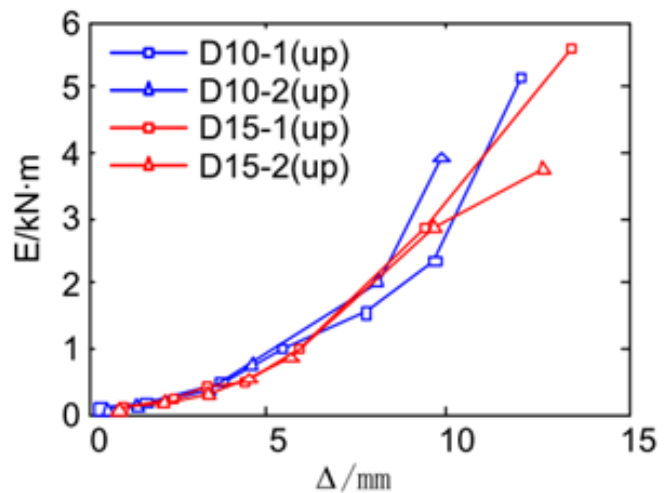


Figure 22. Specimens' energy consumption based on quasi-static test results.

15% eccentricity, the assumption is valid under gravity and yield load level. Longitudinal rebar violate the assumption because buckling occurs. Therefore, the plane section assumption is more likely verified within a 15% eccentricity ratio.

Experimental results show a reduction in the bending stiffness with the load increment. Results show that the lateral stiffness decrease linearly as the displacement grows. Under the yield load stage, the lateral stiffness is about 60% to 80% of the initial value, under the peak load stage this ratio is only about 40% to 60%, while under the ultimate load stage the value drops to about 20% to 40%.

2.5 Laboratory Test Results Overview

The behavior of the capacity and ductility of the composite megacolumns, with four encased steel sections under combined axial load and bending, has been evaluated with an experimental campaign in two phases. Phase 1 of the study includes six 1:4 scale static tests, and Phase 2 of the study includes four 1:6 scale quasi-static tests.

The two phases result in accordance with the expected results.

The full composite action can be determined during the test, even though the steel sections are not connected to one another. Test results of this test program reveal that the Plane Section Assumption is generally valid for specimens with an $e/h=10\%$ and an $e/h=15\%$, but the interface slip grew with the eccentricity, which suggests that the shear demand is relatively larger for megacolumns.

The concrete core, surrounded by the steel profiles, is highly confined, thus increasing the ductility of the composite column.

Both the static and quasi-static specimens show sufficient deformation capacity. In static tests, the specimens are able to maintain the bending moment at the maximum requirement, while the curvature develops until column failure. In quasi-static tests, the ultimate drift ratios of the specimens meet the minimum requirement specified by the technical specification for concrete structures of tall building in Chinese code (JGJ 3 - 2010).

The code provisions allow the use of reduced stiffness of a concrete member, or composite member, to calculate the first order elastic reaction of the structure. This is a simplified way to account for the second order effect and concrete crack under medium or severe earthquakes. Test results of this program support the conclusion that the stiffness reduction factor can be taken as 0.7 based on the ACI 318 method (the factor is applied to the entire composite cross section) or 0.6 based on the Eurocode 4 method (the factor is applied to the concrete part only).

3.0 Validation of Test Results with FEM and International Codes

This section is dedicated to the comparison between the experimental results, numerical results obtained by FEM models, and the simplified calculation methods based on codes.

3.1 FEM and Chinese JGJ Code Validation

CABR validated the static test results with FEM models and a simplified design method based on Chinese code *JGJ 138-2016: Code for Design of Composite Structures*.

FEM analysis has been completed for both static and quasi-static tests, using the software Abaqus.

For concrete, a damaged plasticity model with a confinement effect is adopted. A tri-linear behavior, with values from the test, is assumed for steel sections and rebar. The concrete and steel sections are simulated by three dimensional eight-node solid elements, and the bars are simulated by two dimensional three-node truss elements. To simplify the model, bars and steel beams are connected with ties to the concrete, so there is no relative displacement or strain difference. The interactions of concrete and steel sections are simulated by nonlinear springs along each dimension (see Figure 23).

Before peak point, the calculated 'axial load vs. vertical displacement' curve follows similar paths to the experimental

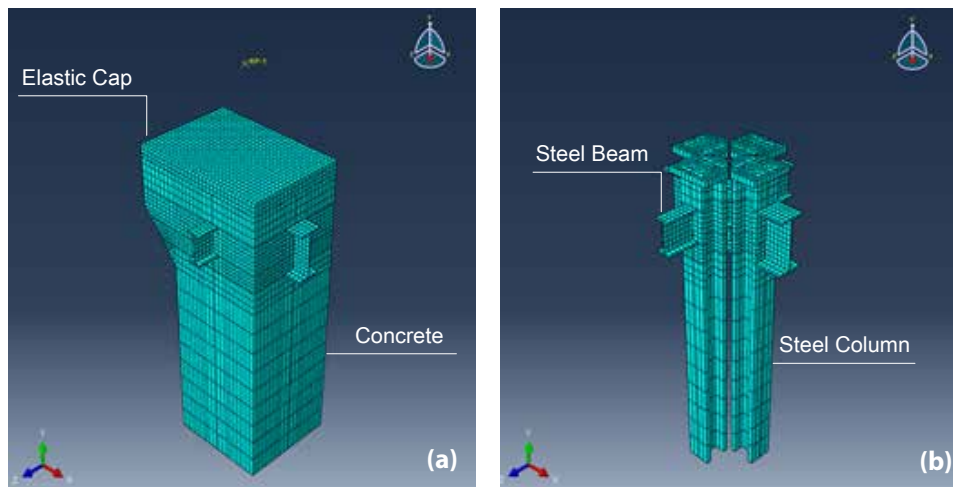


Figure 23. CABR FEM validation of static test in Abaqus concrete mesh (a) and steel section mesh (b). Source: CABR 2015

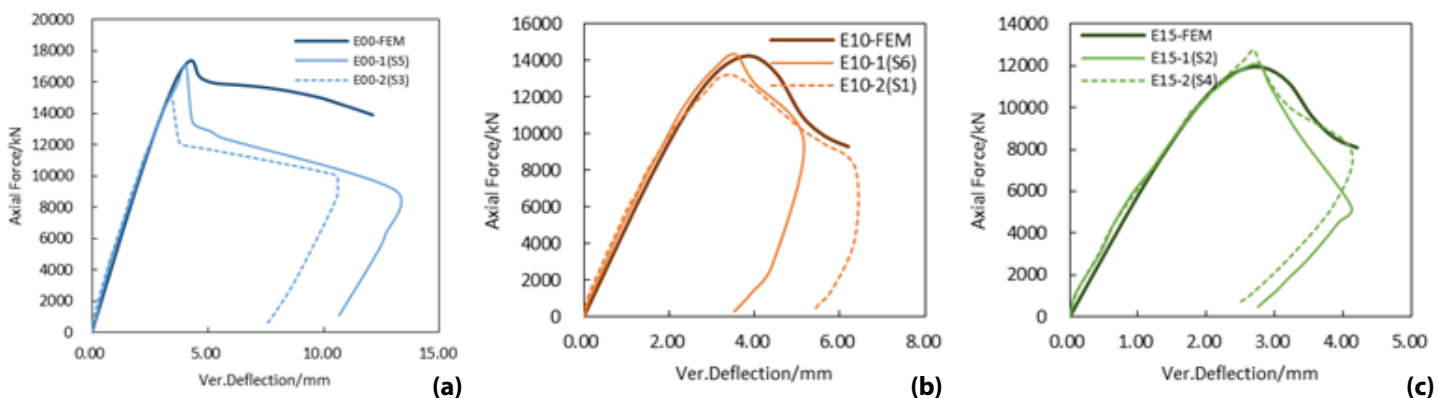


Figure 24. Calculated axial load/vertical deflection curves – E00-1 (a), E10-1 (b), and E15-1 (c). Source: CABR 2015

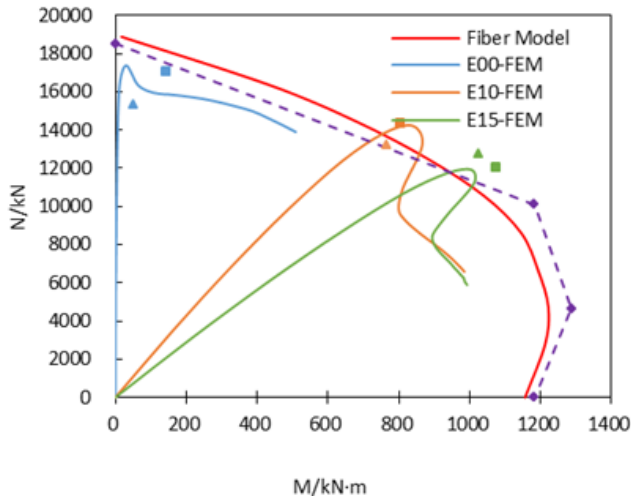


Figure 25. Calculated, FEM and static test interaction curve. Source: CABR 2015

curve. The difference between the curves widen after peak point (see Figure 24).

Once calculated, the FEM models and test interaction curves, presented in Figure 25, show results similar to the capacity of a megacolumn.

Additional deformation and stress distribution findings based on FEM results are detected. Deformations correspond to the experimental data for both purely axial and eccentric specimens.

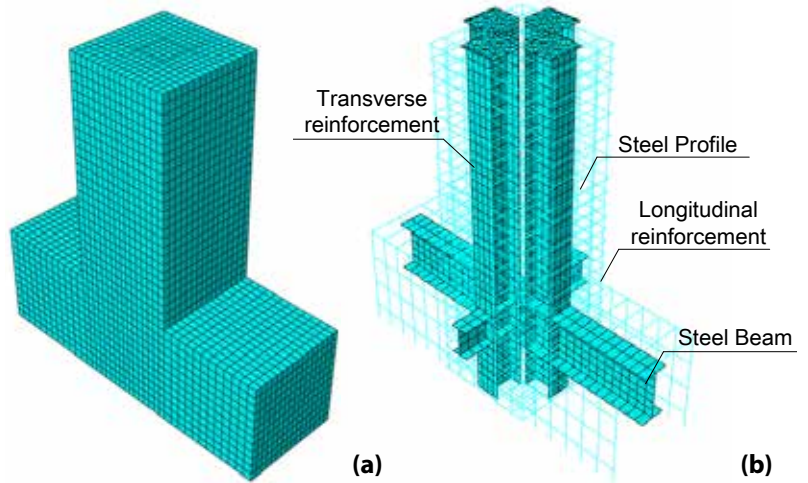


Figure 26. CABR FEM validation of static test in Abaqus – concrete mesh (a) and steel sections mesh (b). Source: CABR 2015

Through the behavior of the springs, additional analyses on shear studs are conducted. The FEM results show that the steel beams play an important role in providing shear resistance along a concrete-steel interface. However, the mechanism may change when the boundary condition changes.

Quasi-static tests have been validated through similar FEM tests, using Abaqus (see Figure 26).

Calculated envelope curves validate the resultant curves from the tests (see Figure 27).

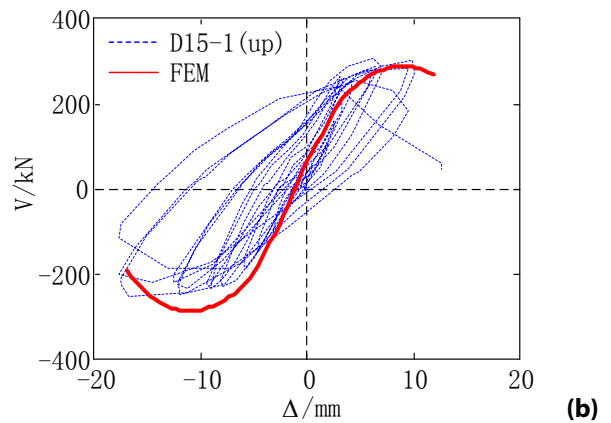
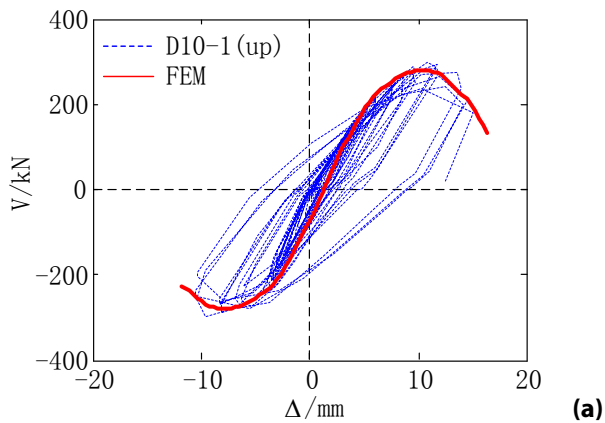


Figure 27. CABR FEM validation of quasi static test envelop curves in Abaqus of the D10-1 upper section (a) and the D15-1 upper section (b). Source: CABR 2015

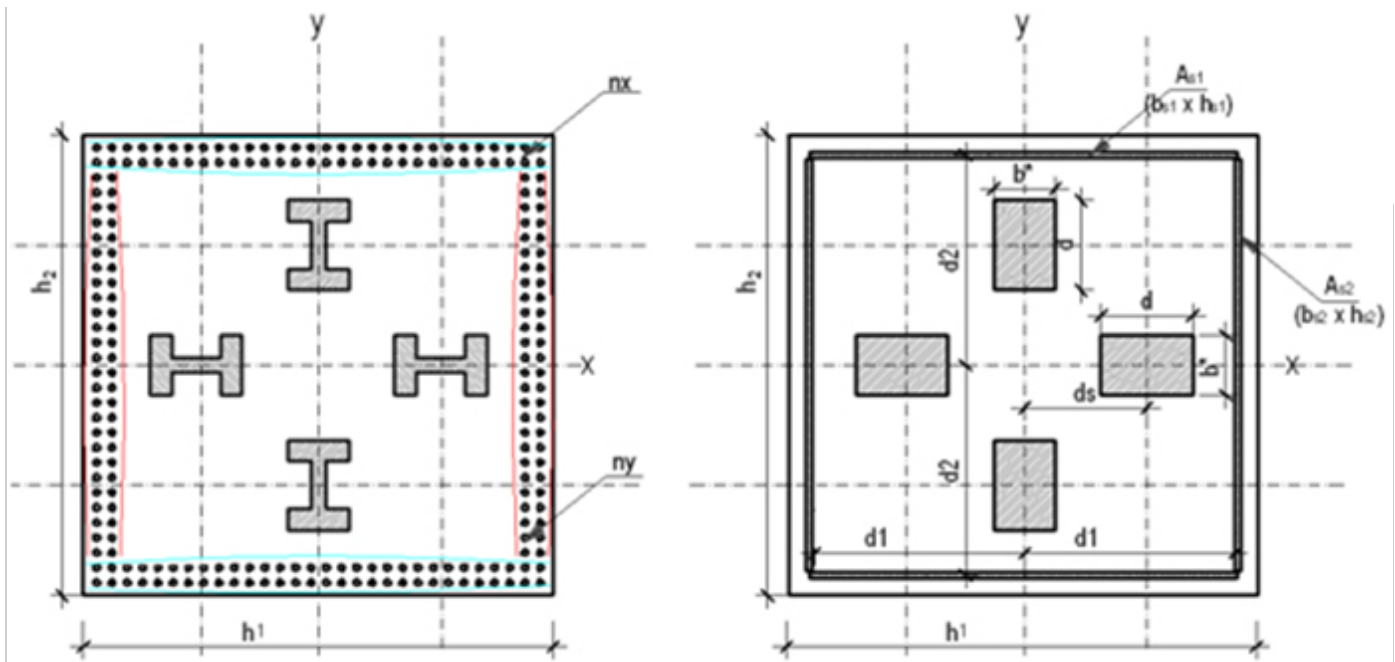


Figure 28. Simplified representation of steel section and rebar equivalent plates.

The interaction curve are close to test results, the axial load, and the bending moment obtained with FEM, with errors ranging from 0.16% to 12.26%.

Based on the test results and on the current Chinese code provision JGJ 138-2016: Code for Design of Composite Structures, a simplified design approach is proposed for a reinforced column with multiple encased steel sections.

Design loads shall be determined based on the first order static analysis. The load factors should be included to amplify the calculated internal forces to obtain sufficient safety. When the factored design loads have been obtained, the bending moment has to be enlarged to account for the member imperfections, additional eccentricities, and the second order effect.

The required calculation of mechanical characteristics of the section (moment of inertia) is based on a simplified representation of the steel rebar and steel section geometry, as equivalent plates and rectangles respectively (see Figure 28).

The factored resistance is calculated based on the nominal resistance, reduced to account for member imperfections, additional eccentricities, and the second order effect.

The JGJ 138 allows the nominal resistance of the composite column calculations, based on the plastic stress distribution of the composite cross sections. A two-step calculation can be used to determine the flexural resistance of the composite cross section:

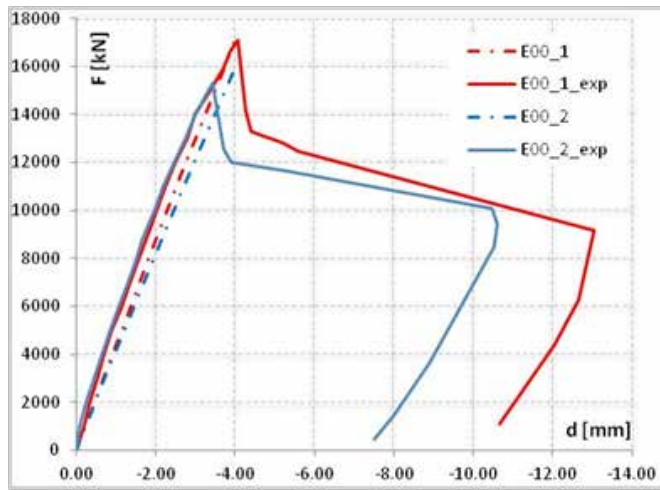
- Step 1: Determine the position of the neutral axis (N.A.) based on the balance condition of the axial load. There are five distinct situations of the position of the N.A.
- Step 2: Calculate the flexural resistance of the composite cross section based on the position of the N.A.

3.2 FEM and Eurocode 4 Validation

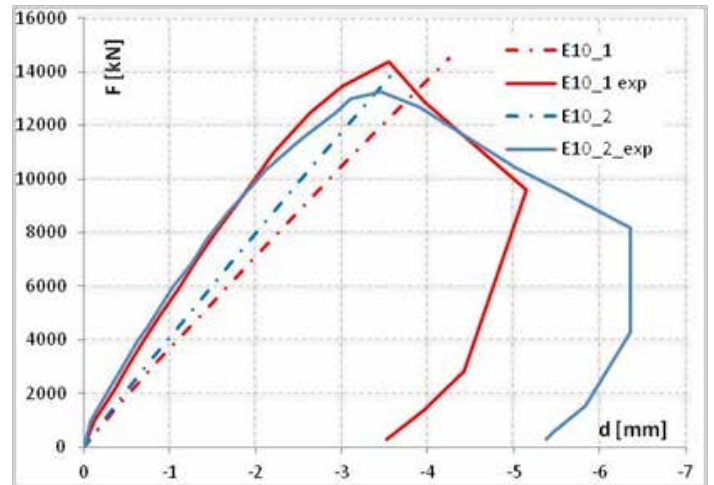
ArcelorMittal carried out the validation of the static test results with FEM models and a simplified design method based on Eurocode 4 (2004) *Design of Composite Steel and Concrete Structures*.

Validation of static test results has been performed with two FEM models, developed with Safir and Abaqus software.

Safir is a computer program that allows modeling of the behavior of building structures. The structure can be made of a 3D skeleton of linear elements such as beams and columns, in



(a)



(b)

Figure 29. Axial load capacity and top displacements comparison between static tests and Abaqus model for E00-1 (a) and E10-1 (b). Source: ArcelorMittal 2015

conjunction with planar elements such as slabs and walls. Different materials, such as steel, concrete, timber, aluminum, gypsum, or thermally insulating products, can be used separately or in combination in the model. The numerical model is a 2D Bernoulli fiber element with 3 nodes and 7 degrees of freedom. This number corresponds to one rotational and two translational DOF for each of the two nodes situated at beam element ends and one relative translational DOF for the node situated at the mid-length of the beam element.

The FEM model in Safir reflects the actual steel and concrete section, the longitudinal layout, and the experimental material characteristics obtained by the test; a perfect bond between concrete and steel is assumed. It can also be assumed that the total length of the specimen will also include the reinforced end extremities, which simulate beam-column joints.

The axial maximum capacity obtained by Safir models are in good accordance with the experimental values of the six specimens. The maximum axial capacity ratios of the two are between 0.85 and 1.19.

On Abaqus models, the specimens are assumed to have a constant cross section. The concrete and the steel sections are simulated by three dimensional eight-node solid elements and the rebar is simulated by two dimensional three-node truss

elements. The interface between concrete and steel profiles is TIE connected, while the rebar is perfectly embedded in the concrete.

The definition of the concrete behavior is based on a concrete damage plasticity model, while a bilinear constitutive model is adopted for the longitudinal bar and the steel profiles.

As shown in Figure 29, Abaqus models' results are in good accordance with the static test results for 0% eccentricity specimens. For eccentric specimens, concrete law influences the behavior of the numerical model; therefore there is a difference in the rigidity. However, the peak values of the axial force are obtained at a similar top displacement.

Static test results have been compared to the results of an extended simplified approach based on Eurocode 4.

As there are no available design standards providing information on how to properly design RC sections with more than one embedded steel profile. The scope is to understand if a simplified code-based approach works for the design of megacolumns as well. The simplified approach applies only to column sections that are symmetrical along two perpendicular axes, uniform along the height of the element.

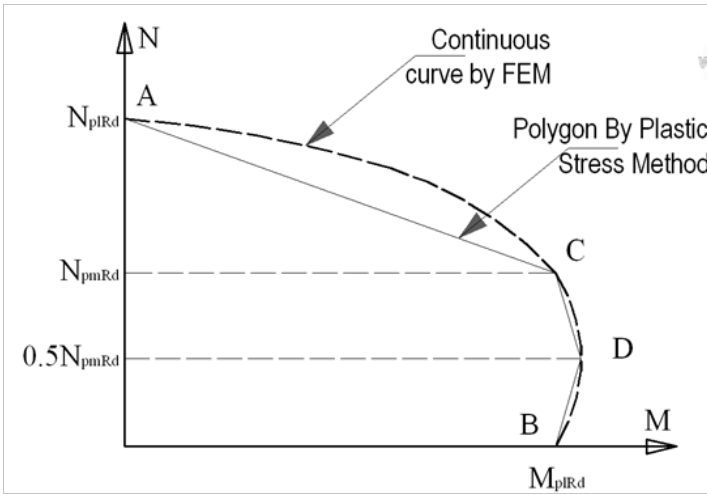


Figure 30. Simplified interaction curve.

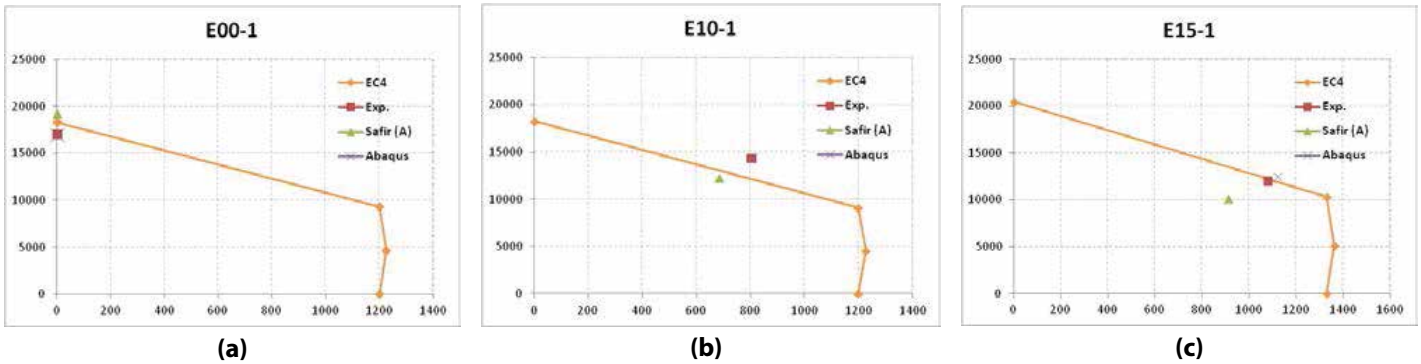


Figure 31. Interaction curve comparison for E00-1 (a), E10-1 (b), and E15-1 (c). Source: ArcelorMittal 2015

The required calculation of mechanical characteristics of the section, the moment of inertia, is based on the simplified representation as presented in Section 3.1.

The simplified interaction curves are therefore represented as a succession of lines joining 4 points, represented as point A, C, D, and B in Figure 30. In this chart, "A" represents the pure compression scenario, "B" is the pure bending scenario, "C" is the pure bending capacity, and "D" is defined as the following:

$$N_D = 0.5 \cdot N_{pm,Rd}$$

$$M_D = M_{max,Rd}$$

Concrete and steel stress blocks are assumed to be rectangular.

In order to have a realistic interaction curve, the buckling effect is taken into account. The principle in which the buckling effects are taken into account is based on different design codes, shown in the design examples and the *Performance and Capacity of Isolated Steel Reinforced Concrete Columns and Design Approaches* report (www.ctbuh.org/megacolumns). This phenomenon of instability lowers the resisting values of the bending moment and axial force. The reduction factor depends on the slenderness, the mechanical characteristic of the section, the direction of buckling, and the ratio between the end moments.

Figure 31 presents a comparison between the adapted simplified method, the experimental results, and the two simplified numerical models created in Abaqus and Safir. These show that a similar result to the experiment is obtained by using the simplified method.

4.0 Simplified Design Methods and Examples

As previously stated, no available design standards provide information on how to properly design reinforced column sections with more than one embedded steel profile.

The research team applied existing methods for design of composite compression members with one encased section based on three main codes to typical sections of megacolumns with four encased steel sections:

1. European code Eurocode 4 (2004): *Design of Composite Steel and Concrete Structures*
2. US AISC 2016 draft version / *ACI 318-14*
3. Chinese code JGJ 138 - 2016: *Code for Design of Composite Structures*

The three listed codes' design methods for composite members are applied to examples of megacolumn sections to demonstrate that code provisions are valid for megacolumns with more than one encased steel section as well.

Megacolumn section layout has been provided by MKA based on actual project requirements for high-rise buildings within China today.

In this section, a simplified method is presented. This allows the calculation of the mechanical properties of the section (moment of inertia and plastic moment) and allows the evaluation of flexural stiffness.

These are necessary for applying the codes.

Please refer to the *Performance and Capacity of Isolated Steel Reinforced Concrete Columns and Design Approaches* report (www.ctbuh.org/megacolumns) for the code application examples.

4.1 Notation

A_a	= area of one steel profile
A_c	= area of concrete shape
A_g	= gross cross-sectional area of composite section
A_s	= total area of the steel profiles
A_{s1}	= equivalent steel plate placed along the x -axis
A_{s2}	= equivalent steel plate placed along the y -axis
A_{sr}	= area of the continuous reinforcing bars
A_{sri}	= cross-sectional area of one reinforcing bar
A_{sr}	= area of continuous reinforcing bars
b	= width of the steel profile
d	= height of the steel profile
b_{s1}	= width of A_{s1} plate, mm
b_{s2}	= width of A_{s2} plate, mm
c_x	= concrete cover, on x - direction
c_y	= concrete cover, on y - direction
d_b	= diameter of the longitudinal reinforcement
d_x	= the distance between the two steel profiles, on y - direction
d_y	= the distance between the two steel profiles on x - direction
d_{sx}	= the distance from the local centroid of the steel profile to the section neutral axis, on x - direction
d_{sy}	= the distance from the local centroid of the steel profile to the section neutral axis, on y - direction
d_{s2x}	= the distance from the local centroid of A_{s1} plate to the section neutral axis, on x - direction
d_{s1y}	= the distance from the local centroid of A_{s2} plate to the section neutral axis, on y - direction
f_{ck}	= characteristic value of compressive cylinder strength of concrete
f_{cd}	= design value of compressive cylinder strength of concrete
f_y	= specified minimum yield stress of steel shape
f_{yd}	= design value of specified minimum yield stress of steel shape
f_{sy}	= yield stress of reinforcing steel
f_{sd}	= design value of yield stress of reinforcing steel

- h_1 = height of the concrete section
 h_2 = width of the concrete section
 h_{s1} = height of A_{s1} plate, mm
 h_{s2} = height of A_{s2} plate, mm
 h_{nx} = distance from centroidal axis (Y-Y) to neutral axis
 I_{cx} = moment of inertia of concrete, about x -axis
 I_x = moment of inertia of one steel shape, about x -axis
 I_y = moment of inertia of one steel shape, about y -axis
 I_{sx} = moment of inertia of steel shapes, about x -axis
 I_{sr1x} = moment of inertia about x axis of A_{s1} plate, mm
 I_{sr2x} = moment of inertia about x axis of A_{s2} plate, mm
 n_x = number of continuous reinforcing bars on x direction
 – corresponding to one horizontal layer
 n_y = number of continuous reinforcing bars on y direction
 – corresponding to one vertical layer
 i = number of rebar layers on A_{s1} equivalent plate
 j = number of rebar layers on A_{s2} equivalent plate
 s_x = spacing between two bars on x direction
 s_y = spacing between two bars on y direction
 n_x = number of bars on x direction on one layer
 n_y = number of bars on y direction on one layer
 n = number of steel profiles oriented on the strong axis
 m = number of steel profiles oriented on the weak axis
 t_f = steel profile flange thickness
 t_w = steel profile web thickness
 Z_{sr1x} = full x -axis plastic modulus of A_{s1} plate, mm
 Z_{sr2x} = full x -axis plastic modulus of A_{s2} plate, mm
 Z_x = full x -axis plastic modulus of one steel shape, mm
 Z_y = full y -axis plastic modulus of one steel shape, mm
 Z_{sx} = full x -axis plastic modulus of entire steel shapes, mm
 Z_{cx} = full x -axis plastic modulus of concrete shape, mm
 Z_{cyn} = x -axis plastic modulus of concrete section within the zone $2h_n$
 Z_{r2xn} = x -axis plastic modulus of A_{s2} plates within the zone $2h_n$
 Z_{cyn} = y -axis plastic modulus of concrete section within the zone $2h_n$
 Z_{r1yn} = y -axis plastic modulus of A_{s1} plates within the zone $2h_n$
 δ = steel contribution ratio
 $\bar{\lambda}$ = the relative slenderness

4.2 Design Case Sections and Properties

The development of a method of calculation for concrete sections, with several encased steel sections, requires the calculation of section characteristics, including the moment of inertia, the plastic moment, the elastic neutral axis, and the plastic neutral axis of huge megacolumn sections. Such calculations can be made through dedicated software, where all the data is given and each reinforcing bar's position and section is defined, or the calculation can be done manually, where it becomes tedious due to the high number of longitudinal bars in megacolumns. In order to facilitate such a calculation, some simplifications are proposed, where the lines of rebar are replaced by equivalent plates. These simplifications have no direct link with the main subject of the paper, which examines design under compression and bending, but they help make user friendly calculations in the design examples presented in this paper and on the shear design of megacolumns.

4.2.1 Flange layers of rebar – moment of inertia

In order to easily make calculations, the layers of rebar, parallel to the neutral axis, can be substituted by an equivalent plate (see Figure 32). The plate area (A_p) can be found with the following equation:

$$A_p = 2n A_b$$

where:

$$A_b = \text{Cross sectional area of one bar}$$

$$n = \text{Number of bars in one layer}$$

The distance of the plate's geometrical center to the neutral axis (d_p) can be found as:

$$d_p = (d_1 + d_2)/2$$

where:

- d_1 = The distance from the center of the first layer of rebar to the neutral axis
 d_2 = The distance from the center of the second layer of rebar to the neutral axis

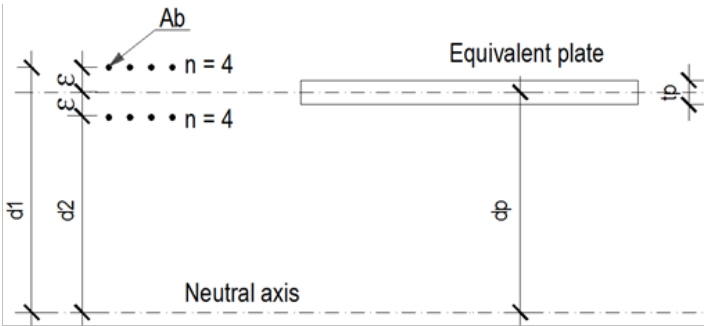


Figure 32: Flange layer of rebar and equivalent plate.

The exact moment of inertia of the reinforcing bars (I_b), which usually neglects the bars own inertia, is equal to:

$$I_b = n A_b (d_1^2 + d_2^2)$$

The inertia of the proposed equivalent plate (I_p), which also neglects the plate own inertia, is equal to:

$$I_p = 2n A_b d_p^2$$

In order to establish to what extent I_p is equivalent to I_b , we express the following:

$$d_1 = d_p + \varepsilon$$

$$d_2 = d_p - \varepsilon$$

Then a comparison is made between the following equations:

$$I_b = 2n A_b (d_p^2 + \varepsilon^2)$$

$$I_p = 2n A_b d_p^2$$

The error is calculated as:

$$\varepsilon^2 / d_p^2$$

It can be considered acceptable if:

$$\varepsilon^2 / d_p^2 < 1\%$$

or if:

$$\varepsilon / d_p < 10\%$$

Expressed with more straightforward data, the following condition can be made:

$$(d_1 - d_2) < 0,2 d_p$$

The condition for an error less than 1% on the moment of inertia of the reinforcing bars, works for a wide range of sections, specifically the section considered in the example presented in this paper. It should be mentioned that the 1% error can induce errors on other parameters, like the complete section stiffness, but this is significantly less than the moment of inertia of reinforcing bars; the error is 0.1% on EI_{eff} in the example.

4.2.2 Flange layers of rebar – plastic moment

With the same symbols as above, the exact plastic moment of rebar layers parallel to the neutral axis is as follows:

$$M_{p,b} = F_{y,b} n A_b (d_1 + d_2)$$

Again neglecting the contribution of the equivalent plate's own plastic moment, the plastic moment due to one plate is equal to:

$$M_{p,b} = F_{y,b} 2 n A_b (d_1 + d_2)/2 = M_{p,b}$$

In this case, the simplification is an exact solution.

4.2.3 Web layers of rebar – moment of inertia

Let us consider a layer of $(n+1)$ bars perpendicular to the neutral axis, where s is the step of bars (see Figure 33).

The total number of bars in one layer is $2n + 1$. The total height (h) of the layer is:

$$h = 2n s$$

A_b is the cross sectional area of one bar.

The exact moment of inertia (I_b) of reinforcing bars is equal to:

$$I_b = 2A_b s^2 (1^2 + 2^2 + \dots + n^2)$$

I_b is found to be equal to:

$$I_b = 2A_b s^2 (2n+1) (n+1) n/6 = (1+1/n) (2n+1) A_b h^2/12$$

In order to make calculations easier, the layers of rebar perpendicular to a considered neutral axis can be substituted by an equivalent plate with the following properties:

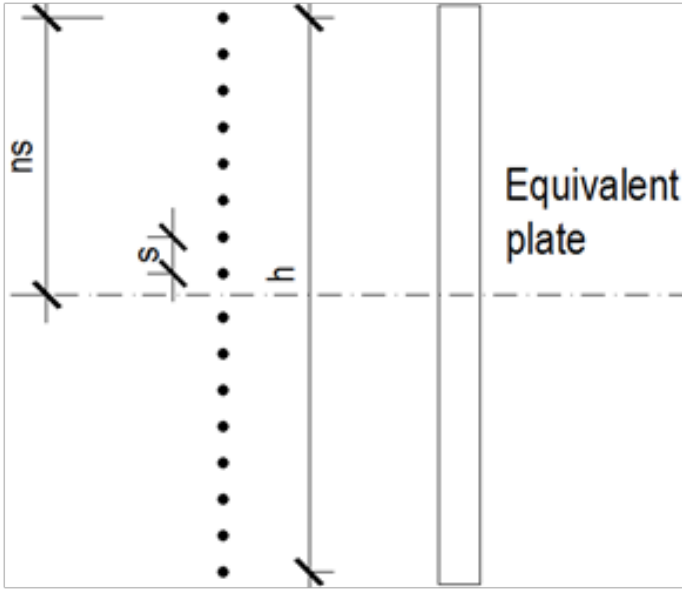


Figure 33. Flange layer of rebar and equivalent plate.

$$A_p = (2n+1)A_b$$

$$h_p = (2n+1)s \quad (\text{Note: } h_p = h + s)$$

$$t_p = (2n+1)A_b / [(2n+1)s] = A_b/s$$

$$I_p = t_p h_p^3 / 12 = (2n+1)A_b h_p^2 / 12 = (1+1/2n)(2n+1) A_b h^2 / 12$$

When comparing I_b and I_p , it appears that the error in using I_p instead of I_b is equal to:

$$(I_b - I_p) / I_p = 1/2n$$

With the example presented in this paper, where $n=12$, the error is $1/(2 \times 12) = 4.2\%$ on the moment of web layers of rebar; as they contribute to only 5.7% to the total section stiffness, the error on the total section stiffness (EI_{eff}) is $0.042 \times 0.057 = 0.0024 = 0.2\%$, which is an acceptable value.

A simple formulation for the acceptability of the simplification would correspond to a 1% error on EI_{eff} . For that situation, the amount of web rebar in a line on one side of the neutral axis should not be less than $1/2n \times 0.1 \leq 0.01$ meaning $n \geq 5$.

This means that the error made on EI_{eff} is less than 1% as long as the amount of web rebars in a line are not less than 10. This is because n is the number of bars for either the top or bottom

equivalent plate. There are 24 web rebars in a line in the example presented in this paper.

4.2.4 Web layers of rebar – plastic moment

With the same notations as above, the exact plastic moment due to web rebars is equal to:

$$M_{p,b} = 2 A_b s (1+2+\dots+n) = n(n+1) A_b s = (n^2 + n) A_b s$$

The plastic moment of the proposed equivalent web plate is equal to:

$$M_{p,p} = t_p h_p^2 / 4 = A_b (2n+1)^2 s^2 / (4s) = (n^2 + n + 1/4) A_b s$$

The error is:

$$1/[4(n^2 + n)]$$

With the minimum s defined in the previous paragraph ($n=10/2=5$), the error is equal to:

$$1/(4 \times 25 + 4 \times 5) = 1/120 = 0.8\%$$

With the number of web rebar in the example presented in this paper, the error is:

$$1/(4 \times 12^2 + 4 \times 12) = 1/120 = 0.1\%$$

4.2.5 Steel profiles – moment of inertia

In order to easily calculate the plastic value of the bending moment of the complete section of the example, where there are four encased HD 400x1299 steel shapes (see Figure 36) and equivalent rectangular plates are replacing the current steel profiles, the rectangular plates have the following dimensions ($d^* \times b^*$), calculated below (see Table 11):

$$d^* = d = 600 \text{ mm}$$

$$b^* = A_s / d^* = 275 \text{ mm}$$

$$I^* = (b^* \times d^{*3}) / 12 = 495000 \times 10^4 \text{ mm}^4$$

where:

d = depth of the steel profile

A_s = one steel profile area

I^{*s} = the moment of inertia of equivalent rectangle

I_{sx} = the moment of inertia of one steel profile

The exact moment of inertia due to four encased steel profiles is:

$$I_{sx} = 4A_s d_{sy}^2 + 4 I_{sx} = 6.258 \times 10^{11} \text{ mm}^4$$

The exact moment of inertia due to four equivalent EI_{eff} rectangular plates is:

$$I_{sx}^* = 4A_s d_{sy}^2 + 4 I^* = 6.1545 \times 10^{11} \text{ mm}^4$$

The difference between the two values is less than 2%. The error on the effective stiffness (EI_{eff}) of the complete section is less than 1%.

4.2.6 Evaluation of effective flexural stiffness

1. European code definitions – EN 1994-1-1

The European code EN 1994-1-1 defines the stiffness of a composite column as having one steel profile, by using the following formula:

$$(EI)_{eff} = E_y \cdot I_y + E_s \cdot I_s + K_e \cdot E_{c,eff} \cdot I_c$$

where:

- $K_e = 0.6$ = The correction factor
- I_y = The second moment of area of the structural section (defined in Table 8 on page 19, and Table 9)
- I_c = The uncracked concrete section (defined in Table 8 on page 19, and 9)
- I_s = The reinforcement (defined in Table 8 on page 19, and 9)

$E_y = 210,000 \text{ MPa}$ = The modulus of elasticity of steel profile (defined by EN 1993-1-1)

$E_{cm} = 22 \cdot \left(\frac{f_{cm}}{10}\right)^{0.3}$ = The modulus of elasticity of the steel profile (defined by EN 1992-1-1)

$E_s = 200,000 \text{ MPa}$ = The modulus of elasticity of reinforcement (defined by EN 1993-1-1)

$$E_{c,eff} = E_{cm} \frac{1}{1 + \left(\frac{N_{G,Ed}}{N_{Ed}}\right) \cdot \varphi_t}$$

Where φ_t is the creep coefficient according to EN 1992-1-1, 3.1.4 or 11.3.3, which depends on the age (t) of the concrete at the moment considered at the age at loading (t_0). In the experimental campaign case, the value of $\varphi_t = 0$ is:

$$(EI)_{eff} = E_y \cdot I_y + E_s \cdot I_s + 0.6 \cdot E_{cm} \cdot I_c$$

In tall buildings there are significant amounts of long term loads, making up approximately 75% of total loads. Therefore, in the following examples, the normal forces ratio will have the following value:

$$\frac{N_{G,Ed}}{N_{Ed}} = 0.75$$

where:

- N_{Ed} = The total design force
- $N_{G,Ed}$ = The part of the normal force that is permanent

2. US code definitions – AISC 2016

The effective stiffness of a composite section according to AISC LFRD 2016 (I2-6) is:

$$(EI)_{eff} = E_y \cdot I_y + E_s \cdot I_s + C_1 \cdot E_c \cdot I_c$$

where:

$$C_1 = 0.25 + 3 \left(\frac{A_s + A_{sr}}{A_g}\right) \leq 0.7$$

C_1 is the coefficient for the calculation of effective rigidity of an encased composite compression member. For the 1:6 specimens, static experimental campaign, the C_1 factor has the following value:

$$C_1 = 0.25 + 3 \cdot \left(\frac{A_s + A_{sr}}{A_g}\right) = 0.25 + 3 \cdot \left(\frac{21296 \text{ mm}^2 + 1608.5 \text{ mm}^2}{202500 \text{ mm}^2}\right) = 0.589$$

where:

I_y = The second moment of area of the structural steel section (defined in Tables 9 and 10)

I_c = The uncracked concrete section (defined in Tables 9 and 10)

I_s = The un-cracked concrete section and the reinforcement (defined in Tables 9 and 10)

$E_y = E_s = 210,000 \text{ MPa}$ = The modulus of elasticity of steel profile and reinforcement rebars (defined by AISC 2016)

$E_c = 0.043 \cdot w_c^{1.5} \cdot \sqrt{f_c}$ = The modulus of elasticity of the steel profile (defined by AISC 2016)

3) Chinese codes definition – JGJ 138-2016

Rigidity of section steel concrete member and steel pipe concrete column may be calculated according to the following formulas:

$$EI = E_c I_c + E_a I_a$$

$$EA = E_c A_c + E_a A_a$$

$$GA = G_c A_c + G_a A_a$$

where:

$E_c I_c$ and $E_a I_a$ = The section bending rigidity of the reinforced concrete part and the section steel and steel pipe parts, respectively

$E_c A_c$ and $E_a A_a$ = The section axial rigidity of the reinforced concrete part and the section steel and steel pipe parts, respectively

$G_c A_c$ and $G_a A_a$ = The section shear rigidity of the reinforced concrete part and the section steel and steel pipe parts, respectively

For the section steel concrete shear wall without an end column, the axial, bending, and shear rigidity may be approximately calculated according to the concrete shear wall on the same section, and the improving action of the end section steel to the section rigidity may be omitted.

As for the section steel concrete shear wall with an end column, the axial and bending rigidity may be calculated according to the H concrete section; the section steel in the end column may be converted to the equivalent concrete area and counted in the flange area of the H section; and the shear rigidity of wall may not be counted into the section steel action.

As for the steel plate concrete shear wall, the steel plates may be converted to the equivalent concrete area to calculate its axial, bending, and shear rigidity.

The load-bearing capacity of a composite column is evaluated according to the GB 50010-2010 design code. As for reinforced concrete axial compression members, when the stirrups allocated for members meeting the provisions, in Section 9.3 of this code, the normal section compression load-bearing capacity shall meet the following requirements:

$$N \leq 0.9\varphi(f_c A_c + f_y' A_s' + f_a' A_a')$$

(according to JGJ138-2016 (6.2.1-1))

where:

N = The design value of axial compressive force

φ = The stability coefficient of reinforced concrete members (according to Table 6.2.15)

f_c = The design value of concrete axial compressive strength (according to Table 4.1.4-1 of the GB 50010-2010 code)

A_c = The sectional area of concrete shape

A_s' = The sectional area of all longitudinal steel bar

A_a' = The sectional area of all steel sections

In conclusion, we cannot define a stiffness reduction factor according to the Chinese design codes.

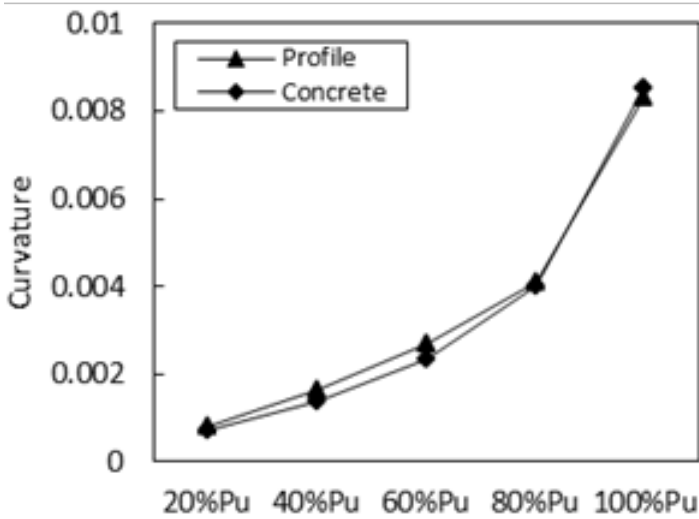
4) Comparison with experimental results

Figures 34 and 35 represent the curvature development of section "A," for specimens E10-1~E15-2. A linear regression is created using points of normal strain versus relative position under a certain load level. The slope of the regressed straight line is taken as the curvature. The curvature of the concrete correlates with that of the steel sections very well and with the validation of Plane Section Assumption it is reliable to

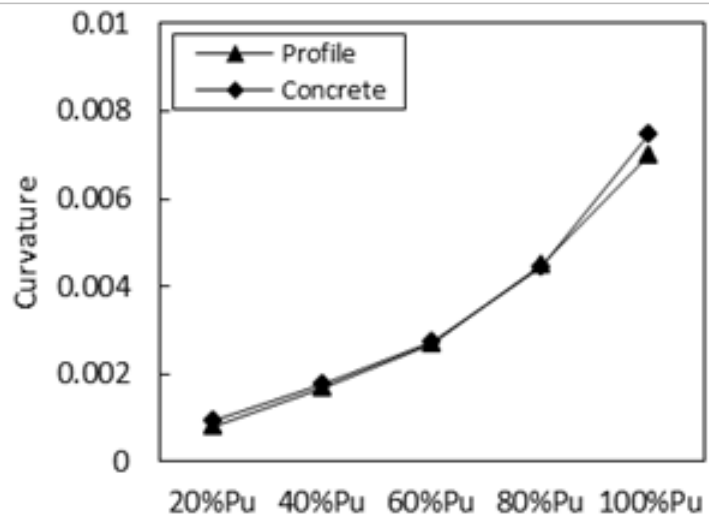
assume the curvatures of different materials on a particular section are the same. Strain gauges that are on the steel sections are more reliable than ones that were on the longitudinal rebar or concrete, so the column curvature can be calculated by normal strain of the steel sections. In addition, it can be observed that the curvature developed more rapidly when the load level was beyond 60%, indicating a reduction in bending stiffness.

The experimental value of the effective flexural stiffness can be determined using the curvature definition of the beam theory. The Euler-Bernoulli beam theory defines the curvature as the following:

$$\chi = \frac{1}{\rho} = \frac{M}{(EI)}$$

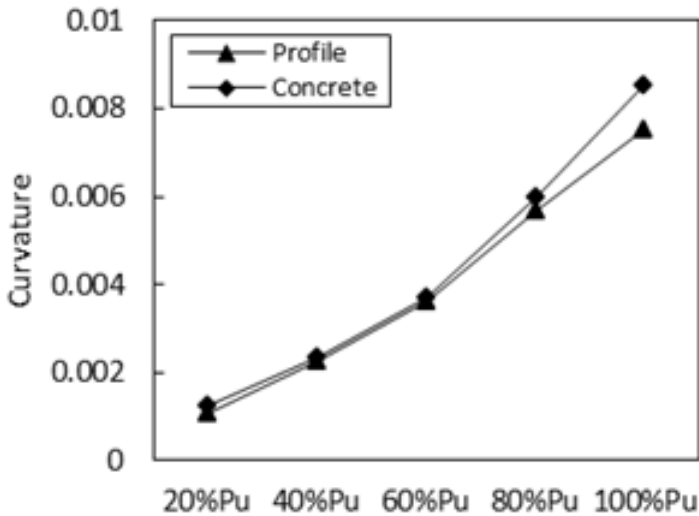


E10-1

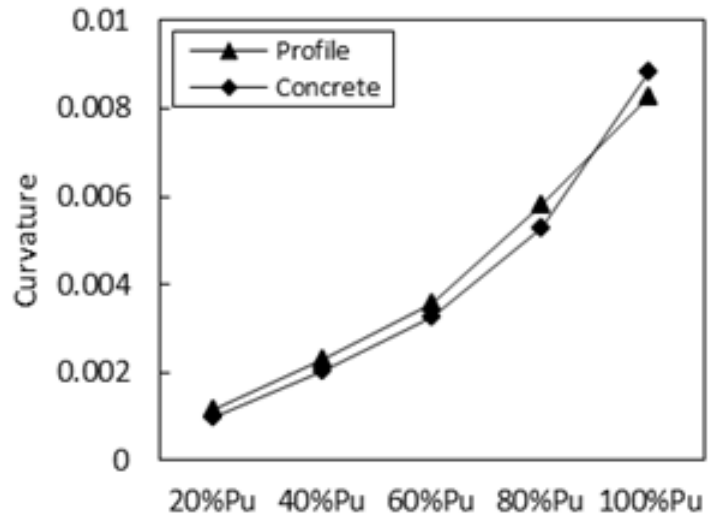


E10-2

Figure 34. Curvature development of section A of specimens E10-1 and E10-2.



E15-1



E15-2

Figure 35. Curvature development of section A of specimens E15-1 and E15-2.

Effective flexural stiffness at 60% Pu

Specimen ID	EI_{eff} Nmm ²			Ratios	
	AISC	EC4	Experimental	AISC/Exp	EC4/Exp
E10-1	1.19E+14	1.23E+14	1.47E+14	81%	84%
E10-2	1.26E+14	1.27E+14	1.50E+14	84%	85%
E15-1	1.23E+14	1.25E+14	1.49E+14	83%	84%
E15-2	1.23E+14	1.26E+14	1.63E+14	75%	77%

Table 9. Specimens E10-1 ~ E15-2 – Effective flexural stiffness – comparison.

where:

- χ = The curvature
- ρ = The radius of curvature

The reduction factor for flexural rigidity can be defined using the following approach:

$$M = (E_y \cdot I_y + E_s \cdot I_s + R_b^k \cdot E_{cm} \cdot I_c) \cdot \chi$$

Each design code defines in particular the modulus of elasticity of the materials, and the calculated values are given in Table 9. A comparison between the experimental values and the theoretical ones has been conducted at two different axial force values, 60% Pu and 100% Pu. The current design of composite columns considers as a maximum

Effective flexural stiffness at maximum load level

Specimen ID	EI_{eff} Nmm ²			Ratios	
	AISC	EC4	Experimental	AISC/Exp	EC4/Exp
E10-1	1.19E+14	1.23E+14	1.26E+14	95%	98%
E10-2	1.26E+14	1.27E+14	1.23E+14	98%	97%
E15-1	1.23E+14	1.25E+14	1.33E+14	92%	94%
E15-2	1.23E+14	1.26E+14	1.21E+14	98%	96%

loading axial value at 60% Pu. At this loading step, the effective flexural stiffness values between the experimental ones and the values defined in the design codes are at least 20% different.

At 100% Pu, it can be observed that the differences in values are under 10%. In conclusion, the methods for the evaluation of effective flexural stiffness developed in the EC4 and AISC design codes can be considered for composite sections reinforced with several steel profiles.

Figure 36 shows the development of the flexural stiffness reduction of the column using the methods presented in the design codes. The rigidity barely reduces before load level 60% Pu, while after 60% Pu the rigidity of the concrete reduces more rapidly than the rigidity of the whole section.

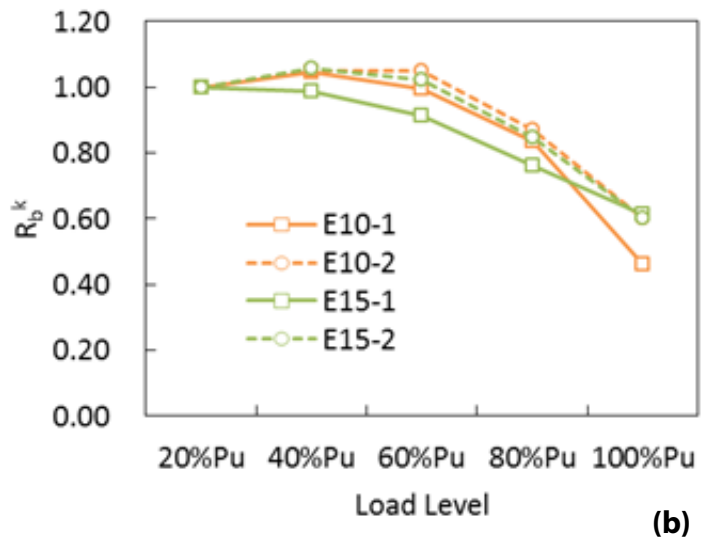
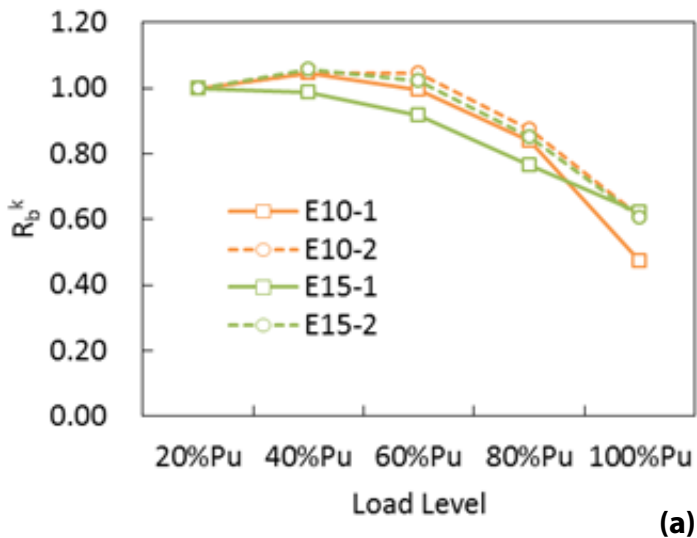


Figure 36. Flexural rigidity degradation of the two design methods – AISC 2016 method (a) and EC4 method (b).

Stiffness reduction factor at 60% Pu

Specimen ID	R_b^k			R_b^k		
	AISC – C_1 value	Experimental	Ratio	EC 4 – K_e value	Experimental	Ratio
E10-1	0.589	0.993	169%	0.6	0.993	166%
E10-2	0.589	1.048	178%	0.6	1.047	175%
E15-1	0.589	0.913	155%	0.6	0.915	153%
E15-2	0.589	1.022	174%	0.6	1.02	170%

Stiffness reduction factor at maximum load level

Specimen ID	R_b^k			R_b^k		
	AISC – C_1 value	Experimental	Ratio	EC 4 – K_e value	Experimental	Ratio
E10-1	0.589	0.64	92%	0.6	0.626	96%
E10-2	0.589	0.567	96%	0.6	0.569	95%
E15-1	0.589	0.638	92%	0.6	0.668	90%
E15-2	0.589	0.571	97%	0.6	0.566	94%

Table 10. Stiffness reduction factors – comparison.

The reduction factors (R_b^k) are determined for each design code with their particular approaches as described in the *Performance and Capacity of Isolated Steel Reinforced Concrete Columns and Design Approaches* report (www.ctbuh.org/megacolumns). The comparisons between the theoretical and experimental values are presented in Table 10, for the axial load values. At 60% Pu loading, the design codes overestimate the R_b^k value, which is at least 50% more. At 100%Pu, good accuracy can be observed for the current design codes, having a difference in value under 10%.

where:

$$R_{b_AISC}^k = \frac{(EI)_{eff_experimental} - E_y \cdot I_y - E_s \cdot I_s}{E_c \cdot I_c}$$

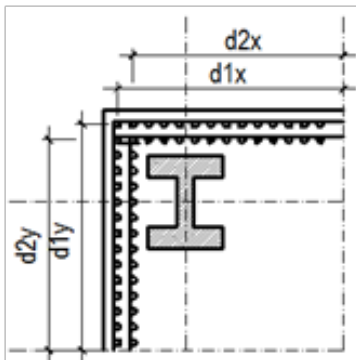
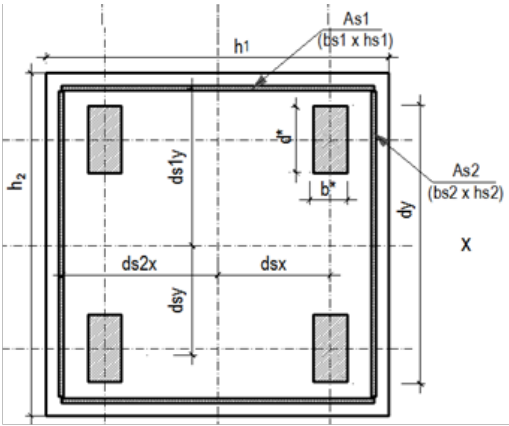
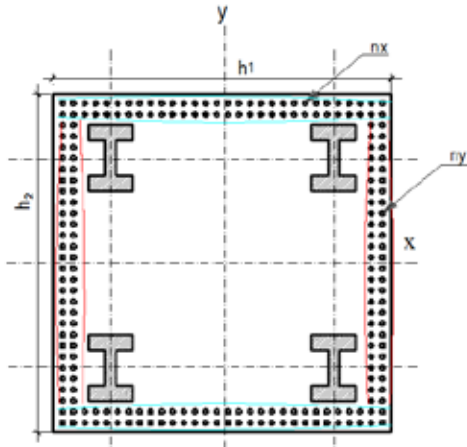
$$R_{b_EC4}^k = \frac{(EI)_{eff_experimental} - E_y \cdot I_y - E_s \cdot I_s}{E_{cm} \cdot I_c}$$

In conclusion, the evaluation of the effective flexural stiffness for composite sections reinforced by different steel profiles can be made by using the formulas in the available design codes.

4.2.7 Tables

A user friendly presentation of the simplifications defined above is given in Table 11, showing different types of cross sections with several embedded steel profiles.

Case of "i" layers of rebar with step "s_x" in x-direction and "j" layers of rebar with step "s_y" in y-direction



Equivalent horizontal plate "nx" rebars on one horizontal layer.

$$A_{s1} = i \cdot n_x \cdot A_{sri} = b_{s1} \cdot h_{s1}$$

$$h_{s1} = (n_x - 1) \cdot s_x$$

$$b_{s1} = \frac{A_{s1}}{h_{s1}}$$

$$d_{s1y} = \sum \frac{d_{yi}}{i}$$

$$Z_{sr1x} = 2 \cdot A_{s1} \cdot d_{s1y}$$

$$I_{sr1x} = 2 \cdot i \cdot n_x \cdot A_{sri} \cdot d_{s1y}^2$$

Equivalent vertical plate "ny" rebars on one vertical layer.

$$A_{s2} = n_y \cdot A_{sri} = b_{s2} \cdot h_{s2}$$

$$h_{s2} = (n_y - 1) \cdot s_y$$

$$b_{s2} = \frac{A_{s2}}{h_{s2}}$$

$$d_{s2x} = \sum \frac{d_{xj}}{j}$$

$$Z_{sr2x} = 2 \cdot \frac{b_{s2} \cdot h_{s2}^2}{4} = \frac{b_{s2} \cdot h_{s2}^2}{2}$$

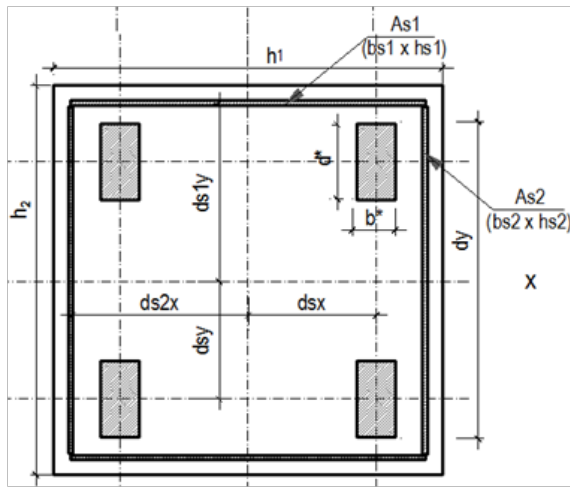
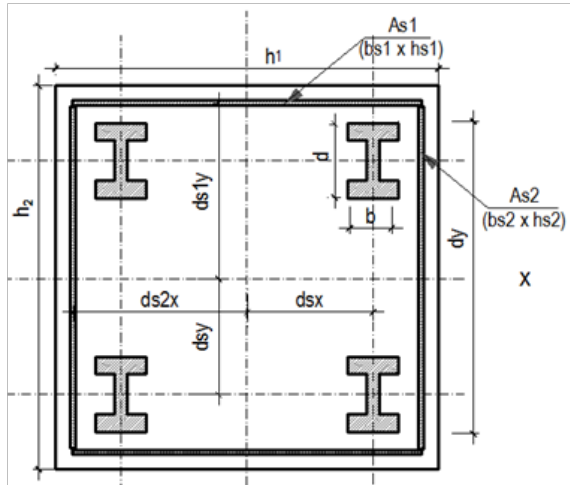
$$I_{sr2x} = 2 \cdot \frac{b_{s2} \cdot h_{s2}^3}{12} = \frac{b_{s2} \cdot h_{s2}^3}{6}$$

Where:

- i – number of rebar layers on A_{s1} equivalent plate
- j – number of rebar layers on A_{s2} equivalent plate
- s_x – spacing between two bars on x direction
- s_y – spacing between two bars on y direction
- n_x – number of bars on x direction on one layer
- n_y – number of bars on y direction on one layer
- d_{siy}, d_{s2x} – distance from the neutral axis of the equivalent plate to the neutral axis of the entire section
- d_{yij}, d_{xj} – distance from the neutral axis of the section to the i^{th} and j^{th} layer of rebar, respectively
- h_{s1} – depth of A_{s1} plate
- b_{s1} – thickness of A_{s1} plate
- h_{s2} – depth of A_{s2} plate
- b_{s2} – thickness of A_{s2} plate
- A_{s1} – area of top (bottom) plate
- A_{s2} – area of lateral plate
- A_{sri} – area of one longitudinal bar
- A_{sr} – total area of longitudinal bars
- Z_{sr1x} – full x-axis plastic modulus of horizontal plates
- Z_{sr2x} – full x-axis plastic modulus of vertical plates
- I_{sr1x} – the moment of inertia of horizontal plates, about the x-axis
- I_{sr2x} – the moment of inertia of vertical plates

Table 11. Definition of plates equivalent to rebar for bending about x-axis.

Case of four steel profiles embedded having the same orientation



$$d^* = d$$

$$b^* = \frac{A_a}{d^*}$$

$$A_s = \sum_{i=1}^n A_a$$

$$Z_{sx} = 4 \cdot A_a \cdot d_{sy}$$

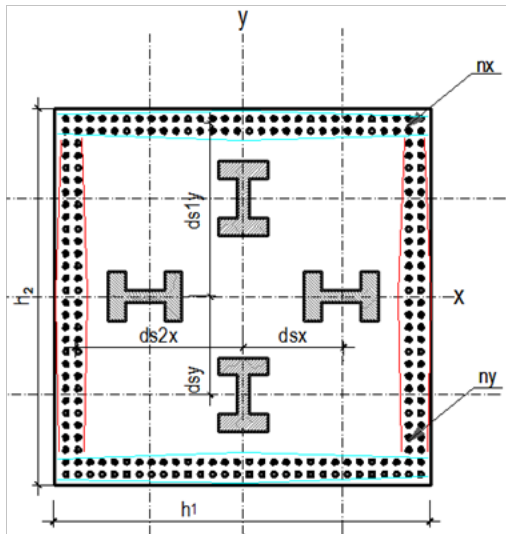
$$I_{sx} = 4 \cdot A_a \cdot d_{sy}^2 + 4 \cdot I_x$$

Where:

- d – steel profile depth
- d^* – equivalent rectangular plate steel depth
- b – steel profile flange width
- b^* – equivalent rectangular plate thickness
- d_{sy} – distance from the neutral axis of the equivalent plate to the neutral axis of the entire section, in the y -direction
- d_{sx} – distance from the neutral axis of the equivalent plate to the neutral axis of the entire section, in the x -direction
- A_a – area of one steel profile
- A_s – total area of steel profiles
- Z_{sx} – static moment of the entire steel shapes, about the x -axis
- I_x – moment of inertia of the steel shape, about the x -axis
- I_{sx} – moment of inertia of the equivalent rectangular plate, about the x -axis

Table 12. Definition of plates equivalent to steel profiles for bending about x -axis.

Case of two profiles oriented on the strong axis and two on the weak axis



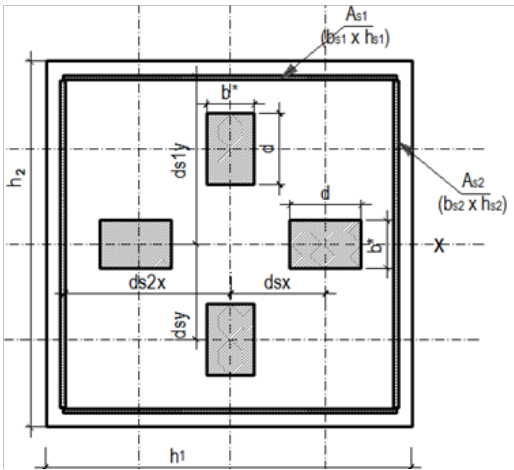
$$d^* = d$$

$$b^* = \frac{A_a}{d^*}$$

$$A_s = \sum_{i=1}^n A_a$$

$$Z_{sx} = 2 \cdot A_a \cdot d_{sy} + 2 \cdot Z_y$$

$$I_{sx} = 2 \cdot A_a \cdot d_{sy}^2 + 2 \cdot I_x$$

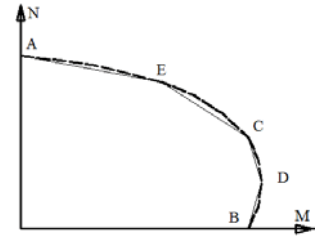


Where:

- d – steel profile depth
- d^* – equivalent rectangular plate steel depth
- b – steel profile flange width
- b^* – equivalent rectangular plate thickness
- d_{sy} – distance from the neutral axis of the equivalent plate to the neutral axis of the entire section, in the y -direction
- d_{sx} – distance from the neutral axis of the equivalent plate to the neutral axis of the entire section, in the x -direction
- A_a – area of one steel profile
- A_s – total area of steel profiles
- Z_y – static moment of the steel shape, about the y -axis
- Z_{sx} – static moment of the entire steel shapes, about the x -axis
- I_x – moment of inertia of the steel shape, about the x -axis
- I_{sx} – moment of inertia of the equivalent rectangular plate, about the x -axis

Table 13. Definition of plates equivalent to profiles having different orientations, for bending about the x -axis.

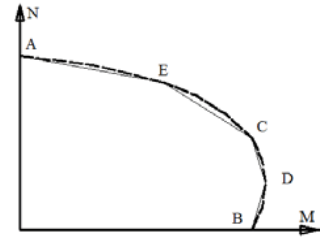
Plastic capacities for a rectangular column with four encased profiles bent about the x-x axis



Section	Stress distribution	Pt.	Defining Equations
	<p>Point A</p> <p>CONCRETE: $0.85f_{cd}$</p> <p>PROFILE: f_{yd}</p> <p>A_{s1} f_{sd}</p> <p>A_{s2} f_{sd}</p>	A	$N_A = A_s \cdot f_{yd} + (A_{s1} + A_{s2}) \cdot f_{sd} + 0.85 \cdot A_c \cdot f_{cd}$ $M_A = 0$
	<p>Point B</p> <p>CONCRETE: $0.85f_{cd}$</p> <p>PROFILE: f_{yd}</p> <p>A_{s1} f_{sd}</p> <p>A_{s2} f_{sd}</p> <p>PNA</p>	B	$N_B = 0$ $M_B = M_{pl.Rd}$
	<p>Point C</p> <p>CONCRETE: $0.85f_{cd}$</p> <p>PROFILE: f_{yd}</p> <p>A_{s1} f_{sd}</p> <p>A_{s2} f_{sd}</p> <p>PNA</p>	C	$N_C = N_{pm.Rd}$ $N_{pm.Rd} = 0.85 \cdot A_c \cdot f_{cd}$ $M_C = M_{pl.Rd}$
	<p>Point D</p> <p>CONCRETE: $0.85f_{cd}$</p> <p>PROFILE: f_{yd}</p> <p>A_{s1} f_{sd}</p> <p>A_{s2} f_{sd}</p> <p>PNA</p>	D	$N_D = 0.5 \cdot N_{pm.Rd}$ $M_{Dx} = M_{max.Rd}$ $M_{max.Rd} = Z_{sx} \cdot f_{yd} + (Z_{r1x} + Z_{r2x}) \cdot f_{sd} + 0.5 \cdot Z_{cx} \cdot (0.85 \cdot f_{cd})$ $Z_{cx} = \frac{h_1 \cdot h_2^2}{4} - Z_{r1x} - Z_{r2x} - Z_{sx}$ <p>Z_{cx} – plastic modulus of concrete shape</p>

Table 14. Composite member with several encased steel profiles, X-X axis anchor points.

Plastic capacities for a rectangular column with four encased profiles bent about the x-x axis



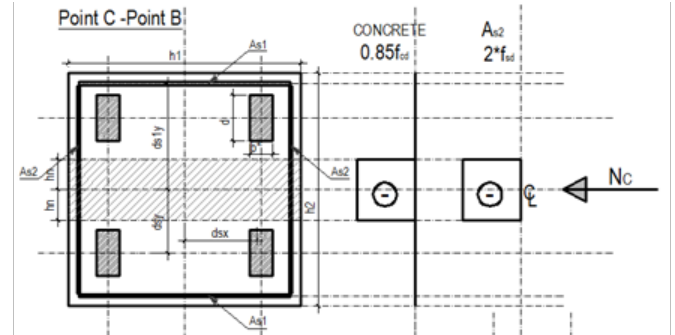
Case 1: h_{nx} between the two profiles $\left(h_{nx} \leq d_{sy} - \frac{d}{2} \right)$:

$$h_{nx} = \frac{N_C}{(2 \cdot h_1 - 4 \cdot b_{s2}) \cdot (0.85 \cdot f_{cd}) + 4 \cdot b_{s2} \cdot f_{sd}}$$

$$Z_{cxn} = h_1 \cdot h_{nx}^2 - Z_{r2xn}$$

$$Z_{r2xn} = 2 \cdot b_{s2} \cdot h_{nx}^2$$

$$M_{pl,Rd} = M_{max,Rd} - Z_{r2xn} \cdot f_{sd} - \frac{1}{2} \cdot Z_{cxn} \cdot (0.85 \cdot f_{cd})$$



Case 2: h_{nx} in the steel profiles $\left(d_{sy} - \frac{d}{2} < h_{nx} \leq d_{sy} + \frac{d}{2} \right)$:

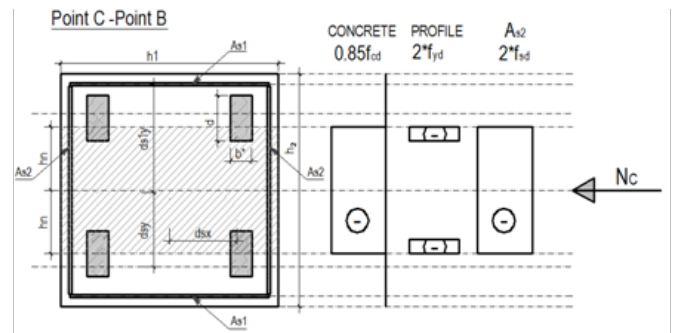
$$Z_{cxn} = h_1 \cdot h_{nx}^2 - Z_{r2xn} - Z_{sxn}$$

$$Z_{sxn} = b^* \cdot \left[h_{nx} - \left(d_{sy} - \frac{d}{2} \right) \right] \cdot \left[3 \cdot h_{nx} + \left(d_{sy} - \frac{d}{2} \right) \right]$$

$$Z_{r2xn} = 2 \cdot b_{s2} \cdot h_{nx}^2$$

$$M_{pl,Rd} = M_{max,Rd} - Z_{r2xn} \cdot f_{sd} - Z_{sxn} \cdot f_{yd} - \frac{1}{2} \cdot Z_{cxn} \cdot (0.85 \cdot f_{cd})$$

$$h_{nx} = \frac{N_C + 4 \cdot \left(d_{sy} - \frac{d}{2} \right) \cdot b^* \cdot (f_{yd} - 0.85 \cdot f_{cd})}{(2 \cdot h_1 - 4 \cdot b^* - 4 \cdot b_{s2}) \cdot (0.85 \cdot f_{cd}) + 4 \cdot b^* \cdot f_{yd} + 4 \cdot b_{s2} \cdot f_{sd}}$$



Case 3: h_{nx} after the two profiles $\left(d_{sy} + \frac{d}{2} < h_{nx} \leq d_{sy} \right)$:

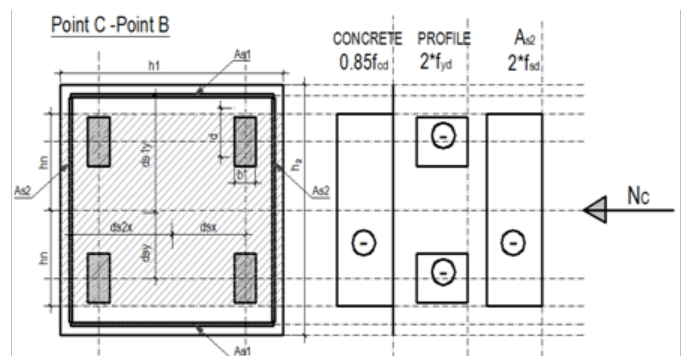
$$h_{nx} = \frac{N_C - 4 \cdot A_a \cdot f_{yd} + 4 \cdot A_a \cdot 0.85 \cdot f_{cd}}{(2 \cdot h_1 - 4 \cdot b_{s2}) \cdot (0.85 \cdot f_{cd}) + 4 \cdot b_{s2} \cdot f_{sd}}$$

$$Z_{cxn} = h_1 \cdot h_{nx}^2 - Z_{r2xn} - Z_{sxn}$$

$$Z_{r2xn} = 2 \cdot b_{s2} \cdot h_{nx}^2$$

$$Z_{sxn} \quad Z_{sx}$$

$$M_{pl,Rd} = M_{max,Rd} - Z_{r2xn} \cdot f_{sd} - Z_{sxn} \cdot f_{yd} - \frac{1}{2} \cdot Z_{cxn} \cdot (0.85 \cdot f_{cd})$$

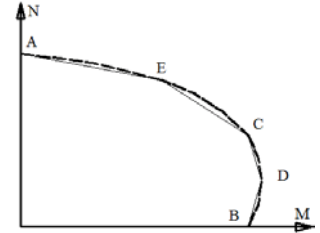


Where:

- Z_{sxn} – x-axis plastic modulus of equivalent steel rectangle bar within the zone $2h_{nx}$
- Z_{cxn} – x-axis plastic modulus of concrete section within the zone $2h_{nx}$
- Z_{r2xn} – x-axis plastic modulus of A_{s2} plate within the zone $2h_{nx}$

Table 15. Evaluation of plastic neutral axis position (h_{nx}) and evaluation plastic bending moment value ($M_{pl,Rd}$) – Example 1.

Plastic capacities for a rectangular column with four encased profiles bent about the x - x axis



Case 1: h_{nx} between the two inner steel profiles ($h_{nx} \leq b^*/2$) :

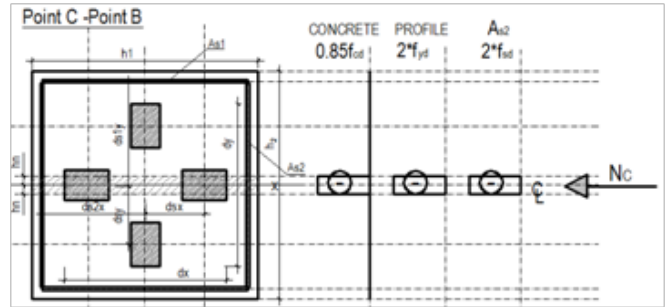
$$h_{nx} = \frac{N_C}{(2 \cdot h_1 - 2 \cdot d - 4 \cdot b_{s2}) \cdot (0.85 \cdot f_{cd}) + 2 \cdot d \cdot f_{yd} + 4 \cdot b_{s2} \cdot f_{sd}}$$

$$Z_{cxn} = h_1 \cdot h_{nx}^2 - Z_{sxn} - Z_{r2xn}$$

$$Z_{r2xn} = 2 \cdot b_{s2} \cdot h_{nx}^2$$

$$Z_{sxn} = 2 \cdot d \cdot h_{nx}^2$$

$$M_{plRd} = M_{max,Rd} - Z_{sxn} \cdot f_{yd} - Z_{r2xn} \cdot f_{sd} - \frac{1}{2} \cdot Z_{cxn} \cdot (0.85 \cdot f_{cd})$$



Case 2: h_{nx} between the profiles ($b^*/2 < h_{nx} \leq d_{sy} - d/2$) :

$$h_{nx} = \frac{N_C + 2 \cdot A_a \cdot 0.85 \cdot f_{cd} - 2 \cdot A_a \cdot f_{yd}}{(2 \cdot h_1 - 4 \cdot b_{s2}) \cdot (0.85 \cdot f_{cd}) + 4 \cdot b_{s2} \cdot f_{sd}}$$

$$Z_{r2xn} = 2 \cdot b_{s2} \cdot h_{nx}^2$$

$$Z_{cxn} = h_1 \cdot h_{nx}^2 - Z_{r2xn} - Z_{sxn}$$

$$Z_{sxn} = 2 \cdot Z_y$$

$$M_{plRd} = M_{max,Rd} - Z_{sxn} \cdot f_{yd} - Z_{r2xn} \cdot f_{sd} - \frac{1}{2} \cdot Z_{cxn} \cdot (0.85 \cdot f_{cd})$$

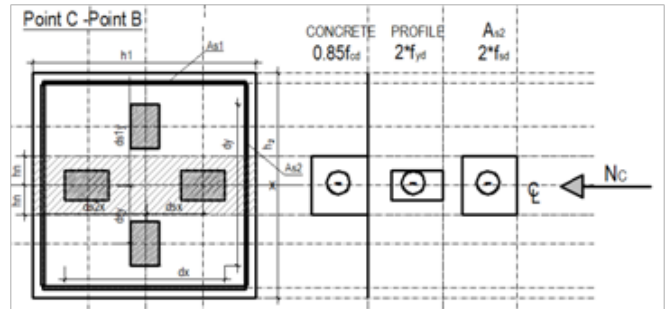


Table 16. Evaluation of plastic neutral axis position (h_{nx}) and evaluation plastic bending moment value (M_{plRd}) – Example 2.

Case 3: h_{nx} placed in the outer steel profiles $\left(d_{sy} - \frac{d}{2} < h_{nx} \leq d_{sy} + \frac{d}{2} \right)$:

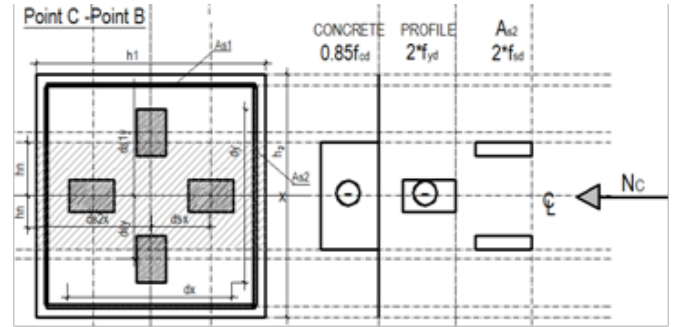
$$h_{nx} = \frac{N_C + 2 \cdot A_a \cdot 0.85 \cdot f_{cd} - 2 \cdot (d_{sy} - \frac{d}{2}) \cdot b^* \cdot 0.85 \cdot f_{cd} + 2 \cdot (d_{sy} - \frac{d}{2}) \cdot b^* \cdot f_{yd} - 2 \cdot A_a \cdot f_{yd}}{(2 \cdot h_1 - 2 \cdot b^* - 4 \cdot b_{s2}) \cdot (0.85 \cdot f_{cd}) + 2 \cdot b^* \cdot f_{yd} + 4 \cdot b_{s2} \cdot f_{sd}}$$

$$Z_{cxn} = h_1 \cdot h_{nx}^2 - Z_{r2xn} - Z_{sxn}$$

$$Z_{r2xn} = 2 \cdot b_{s2} \cdot h_{nx}^2$$

$$Z_{sxn} = 2 \cdot Z_y + \frac{b^*}{2} \cdot \left[h_{nx} - \left(d_{sy} - \frac{d}{2} \right) \right] \cdot \left[3 \cdot h_{nx} + \left(d_{sy} - \frac{d}{2} \right) \right]$$

$$M_{pl,Rd} = M_{max,Rd} - Z_{r2xn} \cdot f_{sd} - Z_{sxn} \cdot f_{yd} - \frac{1}{2} \cdot Z_{cxn} \cdot (0.85 \cdot f_{cd})$$



Case 4: For h_{nx} between the two extreme profiles and the rebars $\left(d_{sy} + \frac{d}{2} < h_{nx} \leq d_{sy} \right)$

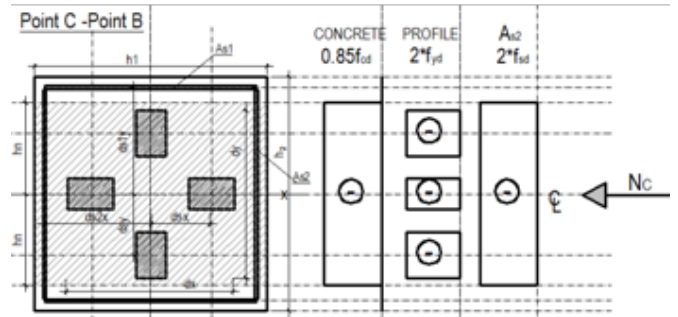
$$h_{nx} = \frac{N_C + 2 \cdot A_a \cdot 0.85 \cdot f_{cd} - 2 \cdot (d_{sy} - \frac{d}{2}) \cdot b^* \cdot 0.85 \cdot f_{cd} + 2 \cdot (d_{sy} - \frac{d}{2}) \cdot b^* \cdot f_{yd} - 2 \cdot A_a \cdot f_{yd}}{(2 \cdot h_1 - 2 \cdot b^* - 4 \cdot b_{s2}) \cdot (0.85 \cdot f_{cd}) + 2 \cdot b^* \cdot f_{yd} + 4 \cdot b_{s2} \cdot f_{sd}}$$

$$Z_{cxn} = h_1 \cdot h_{nx} - Z_{r2xn} - Z_{sxn}$$

$$Z_{r2xn} = 2 \cdot b_{s2} \cdot h_{nx}^2$$

$$Z_{sxn} = 2 \cdot Z_y + \frac{b^*}{2} \cdot \left[h_{nx} - \left(d_{sy} - \frac{d}{2} \right) \right] \cdot \left[3 \cdot h_{nx} + \left(d_{sy} - \frac{d}{2} \right) \right]$$

$$M_{pl,Rd} = M_{max,Rd} - Z_{r2xn} \cdot f_{sd} - Z_{sxn} \cdot f_{yd} - \frac{1}{2} \cdot Z_{cxn} \cdot (0.85 \cdot f_{cd})$$

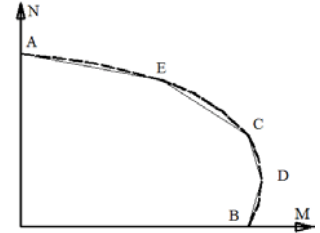


Where:

- Z_{sxn} – x-axis plastic modulus of equivalent steel rectangle bar within the zone $2h_{nx}$
- Z_{cxn} – x-axis plastic modulus of concrete section within the zone $2h_{nx}$
- Z_{r2xn} – x-axis plastic modulus of A_{s2} plate within the zone $2h_{nx}$

Table 16. Evaluation of plastic neutral axis position (h_{nx}) and evaluation plastic bending moment value ($M_{pl,Rd}$) – Example 2 (continued).

Plastic capacities for a rectangular column with six encased profiles bent around the x - x axis



Case 1: h_{nx} between the two inner steel profiles ($h_{nx} \leq d/2$) :

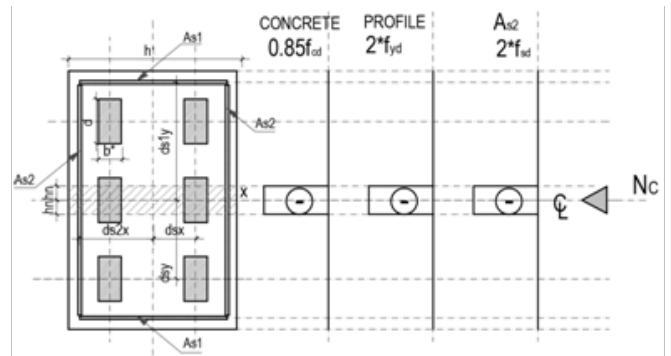
$$h_{nx} = \frac{N_C}{(2 \cdot h_1 - 4 \cdot b^* - 4 \cdot b_{s2}) \cdot (0.85 \cdot f_{cd}) + 4 \cdot b^* \cdot f_{yd} + 4 \cdot b_{s2} \cdot f_{sd}}$$

$$Z_{cxn} = h_1 \cdot h_{nx}^2 - Z_{sxn} - Z_{r2xn}$$

$$Z_{r2xn} = 2 \cdot b_{s2} \cdot h_{nx}^2$$

$$Z_{sxn} = 2 \cdot b^* \cdot h_{nx}^2$$

$$M_{plRd} = M_{max.Rd} - Z_{sxn} \cdot f_{yd} - Z_{r2xn} \cdot f_{sd} - \frac{1}{2} \cdot Z_{cxn} \cdot (0.85 \cdot f_{cd})$$



Case 2: h_{nx} between the profiles ($d/2 < h_{nx} \leq d_{sy} - d/2$) :

$$h_{nx} = \frac{N_C + 2 \cdot A_a \cdot 0.85 \cdot f_{cd} - 2 \cdot A_a \cdot f_{yd}}{(2 \cdot h_1 - 4 \cdot b_{s2}) \cdot (0.85 \cdot f_{cd}) + 4 \cdot b_{s2} \cdot f_{sd}}$$

$$Z_{r2xn} = 2 \cdot b_{s2} \cdot h_{nx}^2$$

$$Z_{cxn} = h_1 \cdot h_{nx}^2 - Z_{r2xn} - Z_{sxn}$$

$$Z_{sxn} = 2 \cdot Z_x$$

$$M_{plRd} = M_{max.Rd} - Z_{sxn} \cdot f_{yd} - Z_{r2xn} \cdot f_{sd} - \frac{1}{2} \cdot Z_{cxn} \cdot (0.85 \cdot f_{cd})$$

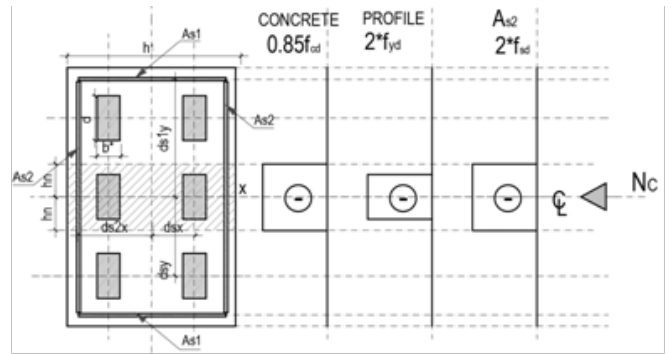


Table 17. Evaluation of plastic neutral axis position (h_{nx}) and evaluation plastic bending moment value (M_{plRd}).

Case 3: h_{nx} placed in the outer steel profiles $(d_{sy} - d/2 < h_{nx} \leq d_{sy} + d/2)$

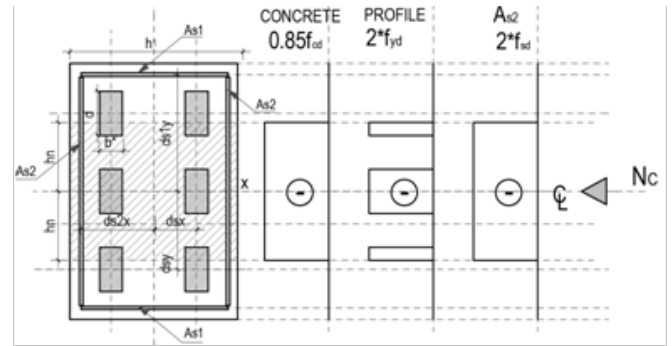
$$h_{nx} = \frac{N_C + 2 \cdot A_a \cdot 0.85 \cdot f_{cd} - 4 \cdot (d_{sy} - d/2) \cdot b^* \cdot 0.85 \cdot f_{cd} - 2 \cdot A_a \cdot f_{yd} + 4 \cdot (d_{sy} - d/2) \cdot b^* \cdot f_{yd}}{(2 \cdot h_1 - 4 \cdot b^* - 4 \cdot b_{s2}) \cdot (0.85 \cdot f_{cd}) + 4 \cdot b^* \cdot f_{yd} + 4 \cdot b_{s2} \cdot f_{sd}}$$

$$Z_{cxn} = h_1 \cdot h_{nx}^2 - Z_{r2xn} - Z_{sxn}$$

$$Z_{r2xn} = 2 \cdot b_{s2} \cdot h_{nx}^2$$

$$Z_{sxn} = 2 \cdot Z_x + 2 \cdot b^* \cdot \left[h_{nx} - \left(d_{sy} - \frac{d}{2} \right) \right] \cdot \left[h_{nx} + \left(d_{sy} - \frac{d}{2} \right) \right]$$

$$M_{pl,Rd} = M_{max,Rd} - Z_{r2xn} \cdot f_{sd} - Z_{sxn} \cdot f_{yd} - \frac{1}{2} \cdot Z_{cxn} \cdot (0.85 \cdot f_{cd})$$



Case 4: For h_{nx} between the two extreme profiles and the rebars $(d_{sy} + d/2 < h_{nx} \leq d_{sy})$

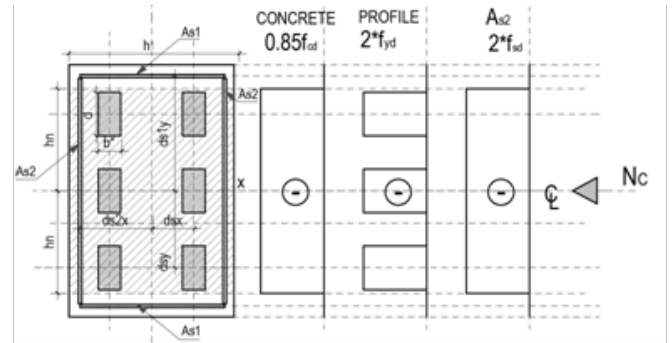
$$h_{nx} = \frac{N_C - 4 \cdot A_a \cdot f_{yd} + 4 \cdot A_a \cdot 0.85 \cdot f_{cd}}{(2 \cdot h_1 - 4 \cdot b_{s2}) \cdot (0.85 \cdot f_{cd}) + 4 \cdot b_{s2} \cdot f_{sd}}$$

$$Z_{cxn} = h_1 \cdot h_{nx}^2 - Z_{r2xn} - Z_{sxn}$$

$$Z_{r2xn} = 2 \cdot b_{s2} \cdot h_{nx}^2$$

$$Z_{sxn} = Z_{sx}$$

$$M_{pl,Rd} = M_{max,Rd} - Z_{r2xn} \cdot f_{sd} - Z_{sxn} \cdot f_{yd} - \frac{1}{2} \cdot Z_{cxn} \cdot (0.85 \cdot f_{cd})$$



Where:

- Z_{sxn} – x-axis plastic modulus of equivalent steel rectangle bar within the zone $2h_{nx}$
- Z_{cxn} – x-axis plastic modulus of concrete section within the zone $2h_{nx}$
- Z_{r2xn} – x-axis plastic modulus of A_{s2} plate within the zone $2h_{nx}$

Table 17. Evaluation of plastic neutral axis position (h_{nx}) and evaluation plastic bending moment value ($M_{pl,Rd}$) (continued).

5.0 Conclusions

The results of the static and quasi-static tests on reinforced columns with four encased steel sections have been validated with FEM methods and compared with simplified code provision methods.

The simplified methods provided by codes are generally valid for composite compression members with one steel encased section. However, research program results show that code provisions are valid also for megacolumns with more than one encased steel section.

1. Simplified design approaches are proposed and described in this report in accordance with Chinese codes JGJ 138. The design approaches are applicable to megacolumns within a 15% eccentricity ratio.
2. A new extended method based on Eurocode 4 and AISC design has been developed in order to design the composite columns with several steel profiles embedded. The method is an extension of the Plastic Distribution Method and takes into account all the assumptions that are defined in EC 4 – Clause 6.7. Two numerical models have been created in order to simulate the behavior of experimental tests. Comparing the adapted simplified method and the two simplified numerical models created in Abaqus and Safir, similar results to the experimental part are obtained.

The Adapted Distribution Method N – M interaction diagram has been obtained based on a Plastic Distribution Method

presented in the European design code EC4 and AISC. These expressions have been developed for the cases of composite sections with several encased steel profiles and they are presented in Tables 11 to 17. The simplified method can be used to quickly and easily do a manual evaluation of the axial force-bending moment interaction curve.

3. The current ACI 318, AISC-LRFD, Eurocode 4, and JGJ 138 are evaluated in this test program. For the test specimens, the current codes are able to provide precise predictions on the axial and flexural capacities with sufficient margins of safety.
4. The finite element analyses are conducted as a supplementary to the test research. FEA demonstrated that the interface strength and stiffness influenced the capacity of megacolumns dramatically when subjected lateral loads. This implied that the shear demand on the interfaces became much larger when the steel profiles were separate from one another.

More thoughtful analyses imply that the enhancement in capacity was contributed by both the interface strength and interface stiffness, and that the efficiency of shear studs got smaller as the number of shear studs grew. In a real structure, however, the shear force between the concrete and the steel profiles is contributed by shear studs, bond stress, and friction, but the FEA results only reflect the influence of shear studs. With the existence of bond stress and friction, the influence of shear studs in a real structure may not be as significant as it is shown in the FEA.



References

1. COMPOSITE MEGACOLUMNS WITH ENCASED STEEL SECTIONS: EXPERIMENTAL CAMPAIGN. First methodological report. March – August 2014
2. COMPOSITE MEGACOLUMNS WITH ENCASED STEEL SECTIONS: EXPERIMENTAL CAMPAIGN. Peer reviewers' comments and responses of the research team. November 2014
3. COMPOSITE MEGACOLUMNS WITH ENCASED STEEL SECTIONS: EXPERIMENTAL CAMPAIGN. Third report: August 2014 – July 2015
4. COMPOSITE MEGACOLUMNS WITH ENCASED STEEL SECTIONS: EXPERIMENTAL CAMPAIGN. Final report: December 2015
5. "DESIGN OF COLUMN WITH SEVERAL ENCASED STEEL PROFILES FOR COMBINED COMPRESSION AND BENDING", A. Plumier, T. Bogdan, H. Degèe
6. "DESIGN FOR SHEAR OF COLUMNS WITH SEVERAL ENCASED STEEL PROFILES. A PROPOSAL.", A. Plumier, T. Bogdan, H. Degèe

All references listed above can be requested via email to
Dr. Dario Trabucco, CTBUH Research Manager,
dtrabucco@ctbuh.org

Code References

1. Eurocode 4 (2004): Design of composite steel and concrete structures
2. AISC (2015): Specifications for Structural Steel Buildings – draft version
3. ACI 318-14: Building code requirements for structural concrete
4. Chinese code JGJ 138-2016: Code for Design of Composite Structures

List of Tables

Table 1. Static test selected materials (First Methodological Report, 2014)	11
Table 2. Material strengths for static tests (Units: MPa)	11
Table 3. Vertical and horizontal displacement at ultimate axial load for static test	14
Table 4. Ultimate axial load and bending moment obtained with static tests	15
Table 5. Quasi-static test selected materials	16
Table 6a. Strength of the concrete	16
Table 6b. Strength of steel sections, reinforcement, and shear stud	17
Table 7. Vertical and horizontal displacement at ultimate axial load for quasi-static test	19
Table 8. Ultimate axial load and bending moment obtained with quasi-static tests	19
Table 9. Specimens E10-1~E15-2 – Effective flexural stiffness – comparison	35
Table 10. Stiffness reduction factors – comparison	36
Table 11. Definition of plates equivalent to rebar for bending about x -axis	37
Table 12. Definition of plates equivalent to steel profiles for bending about x -axis	38
Table 13. Definition of plates equivalent to profiles having different orientations, for bending about the x -axis	39
Table 14. Composite member with several encased steel profiles, x - x axis anchor points	40
Table 15. Evaluation of plastic neutral axis position (h_{nx}) and evaluation plastic bending moment value ($M_{pl,Rd}$) – Example 1	41
Table 16. Evaluation of plastic neutral axis position (h_{nx}) and evaluation plastic bending moment value ($M_{pl,Rd}$) – Example 2	42
Table 17. Evaluation of plastic neutral axis position (h_{nx}) and evaluation plastic bending moment value ($M_{pl,Rd}$)	44

List of Figures

Figure 1. Static test specimens' steel layout - longitudinal (Source: CABR 2015)	10
Figure 2. Static test specimens' steel layout - section (Source: CABR 2015)	10
Figure 3. Static test specimens' shear studs layout (Source: CABR 2015)	10
Figure 4. Specimen fabrication – static test (Source: CABR 2015)	11
Figure 5. Static test setup (a), static test boundary condition (b), static test axial load time history (c) (Source: CABR 2015)	12
Figure 6. Static tests setup in lab (Source: CABR 2015)	12
Figure 7. Static test configuration of strain and displacement gages (Source: CABR 2015)	13
Figure 8. Test procedures – 70% of the maximum load (a), after the maximum load (b), and failure mode (c).	13
Figure 9. Crack development of specimens subjected to eccentric loads	14
Figure 10. Theoretical and real interaction curve obtained by static tests	14
Figure 11. Moment vs. rotation of mid-section for eccentric specimens on static test	15
Figure 12. Quasi-static test specimens' steel layout – longitudinal (Source: CABR 2015)	16
Figure 13. Quasi-static test specimens' steel layout – section	16
Figure 14. Quasi-static test specimens' shear stud layout	16
Figure 15. Specimen fabrication – quasi-static test (Source: CABR 2015)	17
Figure 16. The quasi-static test setup and quasi-static boundary condition (a) (b)	17
Figure 17. Quasi-static set up in lab (Source: CABR 2015)	18
Figure 18. Quasi-static test axial load history (a) and the quasi-static test horizontal load history (b)	18
Figure 19. Quasi-static test sensors on the concrete (a), sensors on critical section I (b), and sensors on critical section II (c)	19

Figure 20. Theoretical and real interaction curve obtained by static and quasi-static tests	19
Figure 21. Hysteretic curves for D10-1 (a) and D15-1 (b) specimens	20
Figure 22. Specimens' energy consumption based on quasi-static test results	20
Figure 23. CABR FEM validation of static test in Abaqus concrete mesh (a) and steel section mesh (b) (Source: CABR 2015)	22
Figure 24. Calculated axial load/vertical deflection curves E00-1 (a), E10-1 (b), E15-1 (c) (Source: CABR 2015)	22
Figure 25. Calculated, FEM and static test interaction curve (Source: CABR 2015)	23
Figure 26. CABR FEM validation of static test in Abaqus concrete mesh (a) and steel sections mesh (b) (Source: CABR 2015)	23
Figure 27. CABR FEM validation of quasi static test envelop curves in Abaqus of the D10-1 upper section (a) and the D15-1 upper section (c) (Source: CABR 2015)	23
Figure 28. Simplified representation of steel section and rebar equivalent plates	24
Figure 29. Axial load capacity and top displacements comparison between static tests and Abaqus model for E00-1 (a) and E10-1 (b) (Source: ArcelorMittal 2015)	25
Figure 30. Simplified interaction curve	26
Figure 31. Interaction curve comparison for E00-1 (a), E10-1 (b), and E15-1 (c) (Source: ArcelorMittal 2015)	26
Figure 32. Flange layer of rebar and equivalent plate	30
Figure 33. Flange layer of rebars and equivalent plate.	31
Figure 34. Curvature development of section A of specimens E10-1 and E10-2	34
Figure 35. Curvature development of section A of specimens E15-1 and E152	34
Figure 36. Flexural rigidity degradation of the two design methods	35

There is an ongoing need to optimize construction materials and reduce the size of elements required within the structural systems of high-rise buildings. Minimizing the size of the vertical structural elements, without compromising the economic feasibility of projects, is a persistent challenge of tall building design. The use of composite structural elements, such as combining concrete and steel, along with higher grade materials within each, is a viable solution.

This document is the summary of the research project on composite megacolumns, conducted by CTBUH and the China Academy of Building Research, with assistance from Magnusson Klemencic Associates and sponsorship from ArcelorMittal. Composite megacolumns considered in this research are defined as vertical structural systems that are subject to significant vertical loads and secondary bending moments from wind and seismic actions, with more than one hot-rolled steel section and longitudinal rebar and ties embedded in the concrete. They are believed to be an appropriate solution in terms of structural behavior, cost, and constructability for the design of tall buildings, including towers over 300 meters tall.

A complete description of the present research program, including all information and data of the laboratory testing can be found in the detailed report, titled *Performance and Capacity of Isolated Steel Reinforced Concrete Columns and Design Approaches*, available online at <http://www.ctbuh.org/megacolumns> or through the following QR code:



www.ctbuh.org
www.skyscrapercenter.com



Research funded by:

